Spatiotemporal patterns of street-level solar radiation estimated using Google Street View in a high-density urban environment

Building and Environment 148 (2019) xxx–xxx

Contents lists available at ScienceDirect

Building and Environment

journal homepage: www.elsevier.com/locate/buildenv

Spatiotemporal patterns of street-level solar radiation estimated using Google Street View in a high-density urban environment

Fang-Ying Gong[a,b,*], Zhao-Cheng Zeng[c], Edward Ng[a], Leslie K. Norford[b]

[a] School of Architecture, The Chinese University of Hong Kong, Shatin, NT, Hong Kong
[b] Department of Architecture, Massachusetts Institute of Technology, Cambridge, MA, USA
[c] Division of Geological and Planetary Sciences, California Institute of Technology, Pasadena, CA, USA

ARTICLE INFO

Keywords:
Solar radiation
Sky view factor
Street canyon
Google Street View
Deep learning
Hong Kong

ABSTRACT

This study presents a method for calculating solar irradiance of street canyons using Google Street View (GSV) images and investigates its spatiotemporal patterns in a high-density urban environment. In this method, GSV images provide a unique way to characterize the street morphology from which the diurnal solar path and solar radiation exposure can be estimated in a street canyon. Verifications of our developed method using free-horizon HKO observations and street-level field measurements show that both the calculated clear-sky and all-sky solar irradiance of street canyons well capture the diurnal and seasonal cycles. In the high-density urban areas of Hong Kong, we found that (1) the lowest monthly averaged solar irradiations in winter are 6.6 (December) and 4.6 (February) MJ/m^2/day, and the highest values in summer are 17.3 (July) and 10.8 (June) MJ/m^2/day for clear-sky and all-sky calculations, respectively; (2) The spatial variability of solar irradiation is closely related to sky view factor (SVF). In summer, the irradiation in a low-rise region (SVF≥0.7) on average is about three times that in a high-rise region (SVF≤0.3), and they differ by about five times in winter; (3) Street orientation has a significant impact on the solar radiation received in a high-density street canyon. In general, street canyons with West-East orientation receive higher solar irradiation during summer and lower during winter compared to those with South-North orientation. The generated maps of street-level solar irradiation may help researchers investigate the interactions between solar radiation, human health and urban thermal balance in high-density urban environments.

1. Introduction

Solar radiation is the main driver in regulating urban climate and the street-level thermal energy balance [1]. Solar radiation in urban areas has been extensively investigated in different fields including urban meteorology [2] [3], photovoltaic generation [4] urban heat island effect [5] and such related issues as thermal comfort and human health due to UV exposure [6–8]. Due to the increasing trend in urbanization and an expected warmer climate in the near future, more and more residents are prone to heat stress in cities [9], [10]. Therefore, a better quantification of solar irradiance at the urban street level will greatly improve our understanding of the interactions between radiation, human health and the urban thermal environment.

However, realistic quantification of solar irradiance in street-level urban environments is lacking, because (1) current meteorological sites for measuring solar irradiance are very sparsely located and almost all of them are in free horizon (e.g., Hong Kong Observatory (HKO)); (2) model simulations, which are commonly used for describing solar irradiance under urban geometries, rely heavily on expensive three dimensions (3-D) mapping of cities [4], [11]. However, the street environment in such cities as Hong Kong can be very complex and difficult to be captured by models [12]. In particular, the street tree canopy, a major component of streetscapes, is hard to be parameterized in models; (3) user-made photography, such as fisheye images, offers good detail but is available at only a limited number of locations [13], [14].

In recent years, the street-sensing method has developed to use of publicly and freely accessible street panoramic photographs, e.g. Google Street View (GSV) images, to derive the morphology, including sky view factor (SVF) of street canyons [12], [15–17]. Gong et al. [12] developed an approach to map all street view factors including sky, building, and tree view factors using pyramid scene parsing network (PSPNet), and demonstrated the high accuracy and effectiveness of this method by direct comparison with hemispheric photography. In a high-density urban environment, solar radiation goes into street canyons

* Corresponding author. Room505, AIT Building, School of Architecture, The Chinese University of Hong Kong, Shatin, NT, Hong Kong.
E-mail address: fangying@link.cuhk.edu.hk (F.-Y. Gong).

https://doi.org/10.1016/j.buildenv.2018.10.025
Received 10 July 2018; Received in revised form 12 October 2018; Accepted 12 October 2018
Available online 15 October 2018
0360-1323/

Nomenclature

Symbols

D_{aniso}	Anisotropic diffuse radiation (no clouds) (W/m^2)
D_{aniso_open}	Anisotropic diffuse radiation (no clouds) in free horizon (W/m^2)
D_{cloud}	Diffuse radiation due to cloud (W/m^2)
D_{cloud_open}	Diffuse radiation due to cloud in free horizon (W/m^2)
D_{iso}	Isotropic diffuse radiation (no clouds) (W/m^2)
D_{iso_open}	Isotropic diffuse radiation (no clouds) in free horizon (W/m^2)
D_{open}	Diffuse irradiance on a horizontal surface in free horizon (W/m^2)
D_{street}	Diffuse irradiance on a horizontal surface in a street canyon (W/m^2)
G_0	Global irradiance on a horizontal surface (no clouds) in free horizon (W/m^2)
G_{street}	Global irradiance on a horizontal surface in a street canyon (W/m^2)
E_0	Extraterrestrial radiation (W/m^2)
I_{open}	Direct irradiance on a horizontal surface in free horizon (W/m^2)
I_{street}	Direct irradiance on a horizontal surface in a street canyon (W/m^2)
R^2	Coefficient of determination
T_L	Linke turbidity factor
m_{r0}	Optical air mass
p_0	Normal pressure at sea level (hPa)
f	Binary indicator of the existence of solar ray path obstructions
N	Cloudiness index (octas)
p-value	Significant level
R	Correlation coefficient
p	Local atmospheric pressure (hPa)

Greek symbol

φ	Solar zenith angle (degree)
ψ	Solar azimuth angle (degree)
Ψ_x	View factor for sky, tree, and building when x is specified
Ψ_{sky}	Sky view factor
τ	Transmittance of the direct solar radiation
δ	Solar declination angle
δ_{r0}	Vertical optical thickness of the standard atmosphere
γ	Solar altitude angle (degree)
θ	Polar angle (degree)

Abbreviations

3-D	Three dimensions
API	Application programming interface
BVF	Building view factor
CNN	Convolution neural networks
CUHK	The Chinese University of Hong Kong
GIS	Geographic information system
GSV	Google Street View
H/W	Building-height-to-street-width ratio
HKO	Hong Kong Observatory
PSPNet	Pyramid scene parsing network
SOLPOS	Solar Position and Intensity
SVF	Sky view factor
TVF	Tree view factor
UBL	Urban boundary layer
UHI	Urban heat island
VF	View factor

through their sky opening, while buildings and trees are the two main obstructions of the solar light path that prevents direct sunlight from reaching the ground at particular times of the day. Since GSV images provide a direct mapping of street morphologies, they can be used to quantify the sky opening and the obstructions by building and trees. Moreover, the high-density urban street morphologies, which are usually complex and have large spatial variations, are not well captured by models but can be fully characterized by GSV images. Therefore, extending from our previous work [12], this study proposes using the street geometries characterized using GSV images to quantify the street-

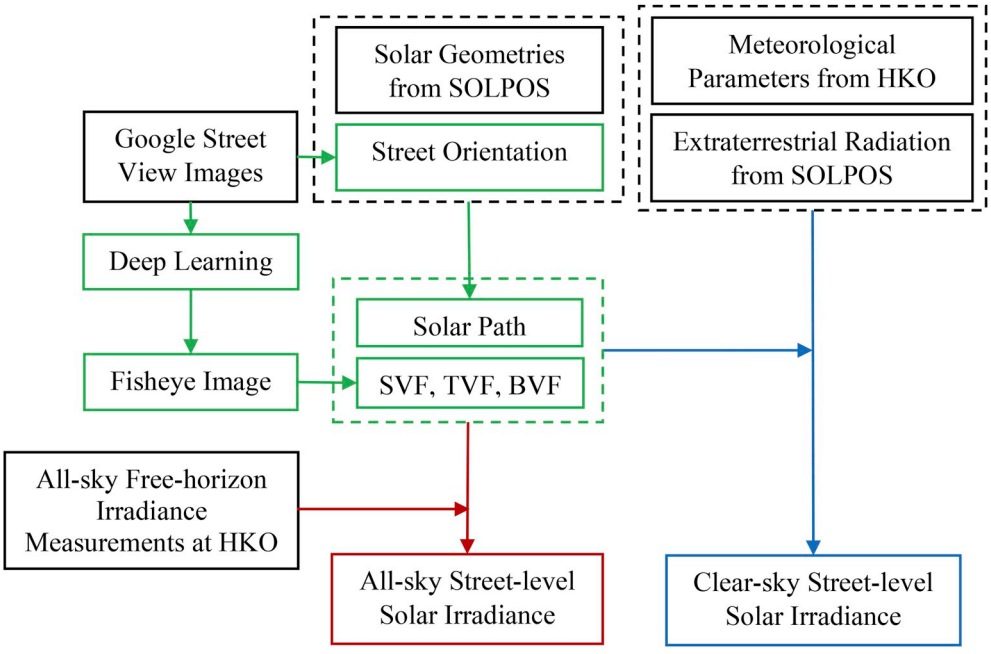

Fig. 1. Schematic framework for this study, in which black rectangles represent the collected datasets, green rectangles represent the calculations of solar path and view factors in street canyons using GSV images, the blue rectangle represents the calculation of clear-sky street-level solar irradiance, and the red rectangle represents the calculation of all-sky street-level solar irradiance in the high-density urban areas of Hong Kong. (For interpretation of the references to colour in this figure legend, the reader is referred to the Web version of this article.)

level solar irradiance in high-density urban areas of Hong Kong. Carrasco-Hernandez et al. [15] investigate the potential of using GSV to quantify street-level total shortwave irradiance. However, their developed method lacks the flexibility for large-scale application. More recently, Middel et al. [18] reported using GSV to calculate the solar hours in New York but solar irradiance was not estimated. Li and Ratti [19] used a statistical ratio, the proportion of direct radiation, to calculate the solar radiation in Boston based on GSV and a 3-D building model, which is expensive and may not always be available elsewhere. The applicability of their method to high-density urban environments is therefore unknown. Moreover, these two studies lack independent verifications of their calculations.

The proposed method in this study is used to map the street-level solar irradiance, including direct and diffuse components, and investigate its spatial and temporal pattern in high-density urban areas of Hong Kong. The advantage of this proposed method is that it doesn't rely on urban 3-D digital models and therefore simplifies the calculation of solar irradiance in street canyons. Since GSV images are available in cities, this method can be applied worldwide to provide a low-cost and effective approach for mapping street-level solar irradiance. The resulted maps of street-level solar irradiance will provide useful datasets for studying the interactions between solar radiation, human health and the urban thermal balance in high-density urban environments.

This paper is outlined as follows. The study area, datasets and methodologies for calculating street-level solar irradiance using GSV images are described in Section 2. Section 3 presents the maps of street-level solar irradiation in the high-density urban areas of Hong Kong and demonstrates its spatial and temporal patterns. This is followed by the discussions in Section 4 and the conclusion in Section 5.

2. Methods

This study aims to develop an approach to calculate the street-level solar irradiance using GSV images and investigates its spatial and temporal patterns in the high-density urban areas of Hong Kong. In this study, we consistently use “solar irradiance” when referring to the intensity of solar radiation (in unit of W/m^2) received by a horizontal surface; and we use “solar irradiation” when referring to the integration of solar irradiance over a certain time range (in unit of MJ/m^2). We also use intensity units, W/m^2, when referring to solar radiation independent of its incidence on a given surface. The methodology framework for this study is presented in Fig. 1 and consists of three main phases. In **Phase I** (green rectangles), the sky, tree and building view factors are first estimated from the GSV images based on our previous study [12] and the diurnal solar path is calculated based on the street and solar geometries; In **Phase II** (blue rectangle), solar irradiance in clear-sky, free horizon conditions is first calculated and then combined with street morphologies and the solar path to derive the clear-sky street-level solar irradiance; In **Phase III** (red rectangle), direct and diffuse components measurements from HKO are used as the all-sky free-horizon solar irradiance and combined with street morphologies and solar path to derive the all-sky street-level solar irradiance.

2.1. Study area and data collection

2.1.1. Study area

Hong Kong is one of the most densely-populated and built-up cities in the world, with a population of over seven million living in around 262 km^2 of developed land [20]. Situated at the coastline of southeastern China (see Fig. 2 (a)) with a subtropical maritime climate, Hong Kong is typically hot and humid in summers while warm in winters [21]. The high-density urban areas of Hong Kong are characterized by high-rise compact building blocks and deep street canyons with building-height-to-street-width (H/W) ratio. In these areas, tall buildings of some 40-60 stories lining narrow streets of 15–25 m width are the norm. Serious issues related to human thermal comfort [22], air pollution [23] and urban heat island effect [24] due to its climate and urban morphologies have been primary planning concerns. As the principal driver of the urban thermal energy balance in street canyons, solar radiation has been widely studied to address these problems [5],

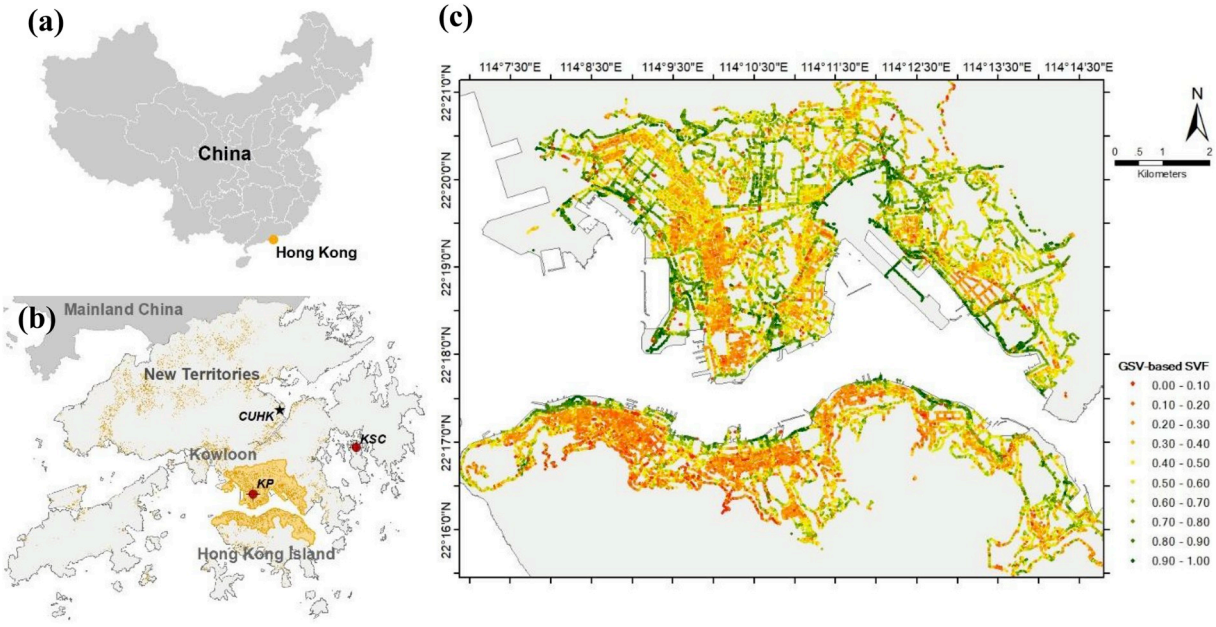

Fig. 2. (a) Location of Hong Kong (yellow circle) in southern coastal region of China; **(b)** High-density urban areas in Hong Kong, as outlined in yellow, including Kowloon and northern Hong Kong Island; The yellow points are the spatial distribution of building footprints; the red points are the locations of King's Park and Kau Sai Chow sites from Hong Kong Observatory; the black star is the location of field measurements in our study (one street canyon of a campus in the urban area of New Territories); **(c)** GSV-based sky view factor map of street canyons derived from 29,264 GSV images along streets at 30-m intervals in the high-density urban areas of Hong Kong [12]. (For interpretation of the references to colour in this figure legend, the reader is referred to the Web version of this article.)

[25–27]. However, progress on the accurate assessment of solar irradiance at street level in high-density urban regions is still limited due to a lack of street-level measurements and sufficient quantifications of street morphologies.

In this study, high-density urban regions of Kowloon and Hong Kong Island are chosen as our study area, as shown in Fig. 2 (b). This area is one of the most densely built and populated areas in the world and has an average building height of 27 m (with a standard deviation of 30.7 m) and the population density of around 42,900 persons per km^2. Fig. 2 (c) shows the spatial distribution of SVF, a direct indicator of street H/W ratio, from Gong et al. [12]. The high-rise, mid-rise and low-rise regions in Hong Kong urban areas can be identified in our study by SVF≤0.3, 0.4≤SVF≤0.6, and SVF≥0.7, respectively, according to local climate zone classification [28]. We can see that most high-rise buildings are distributed in southern and western Kowloon and northern Hong Kong Island.

2.1.2. Data collection

Based on our previous study [12], street panorama images sampled at 30-m intervals are first collected using the GSV Application Programming Interface (API) [29] [30], according to the location (latitude and longitude), horizontal field of view, compass heading, and the vertical angle of the camera relative to the street view vehicle [31]. A total of 26 (width) times 13 (height) tiles are obtained and combined to get a complete panorama image. A total of 33,544 images are collected in the study area. Invalid GSV images, including those with empty content, are filtered out. Examples of GSV images of a typical high-density street canyon are shown in Fig. 3 (a). Differing from Gong et al. [12], in which street orientation is not directly relevant to view factor calculations, the heading of the panorama image is essential for deriving solar path of the street canyon. By default, the vehicle heading direction, which is the center direction of the panorama, can be requested from the Street View Service by providing its latitude and longitude [31]. Eventually, the center heading of the panorama images can be adjusted to the north by shifting the corresponding vehicle heading direction in degrees. The calculation of street view factors in this study refers to the position of the GSV vehicle moving along the roadway which is slightly different from the road axis. Given that most

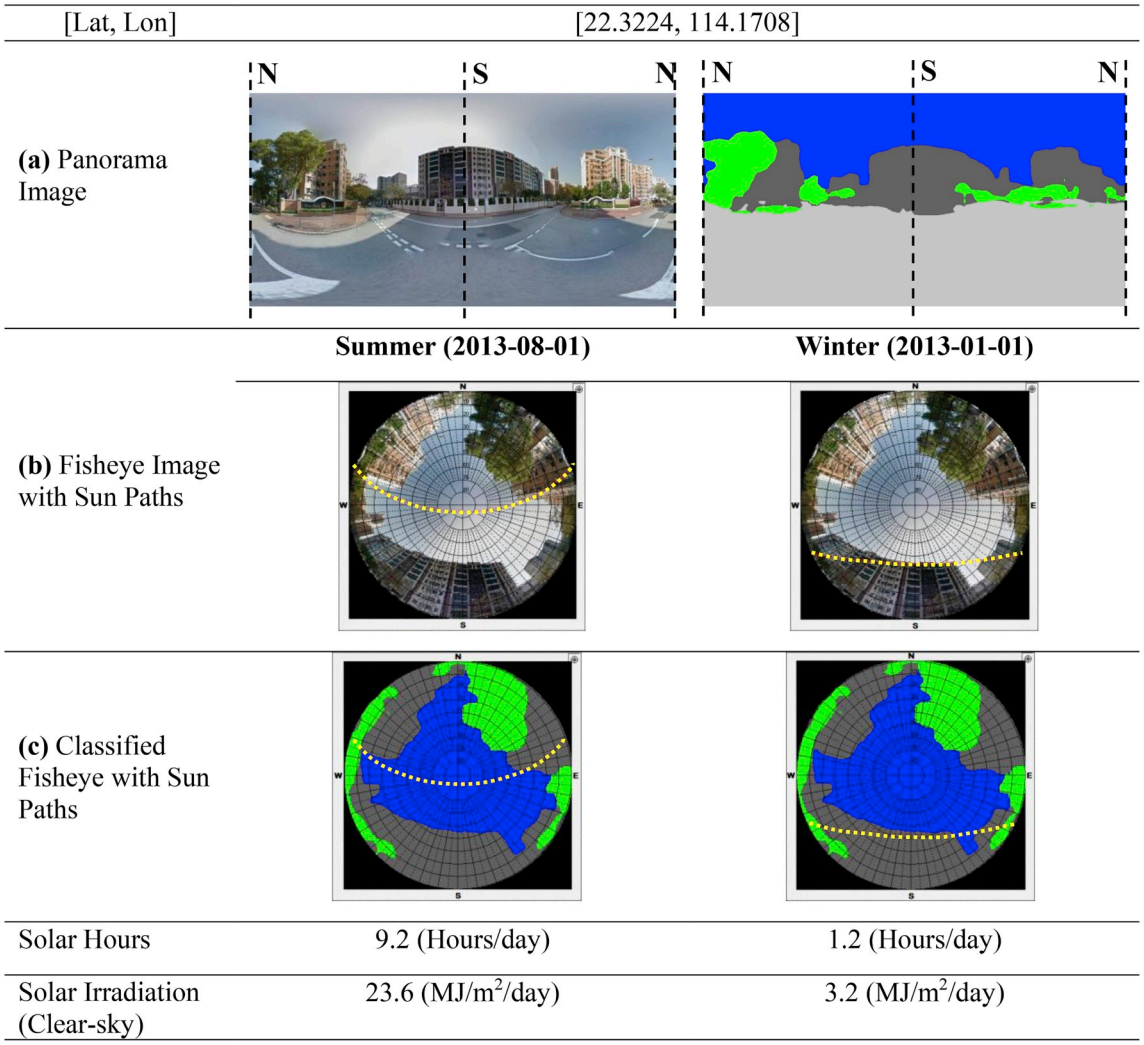

Fig. 3. Workflow for solar irradiance calculation using GSV images shown using an example of a street canyon in high-density urban areas of Hong Kong. **(a)** Panorama image collected using the GSV API, and extractions of sky (in blue), trees (in green), and buildings (in deep grey) using a deep-learning technique. **(b)** Street geometries, including zenith angle indicated by concentric circles and azimuth angle indicated by radius lines, in a fisheye and the overlaid sun paths of summer (August 1st) and winter (January 1st); **(c)** Same as (b) but with classified fisheye images. In addition, clear-sky solar hours and solar irradiation are indicated. (For interpretation of the references to colour in this figure legend, the reader is referred to the Web version of this article.)

streets in Hong Kong have either one lane or two lanes (almost all in high-density urban areas), the axis of the road and the vehicle path are therefore close to each other. So, we assume that the calculation of solar irradiance using GSV is representative for the street axis.

To calculate the solar irradiance, the following meteorological data are obtained: (a) Solar geometries and extraterrestrial radiation. These two datasets can be calculated by the Solar Position and Intensity (SOLPOS) algorithm developed by the National Renewable Energy Laboratory [32]. The algorithm generates the solar position, including solar zenith angle and solar azimuth angle, and extraterrestrial radiation with small uncertainty based on inputs of location, date, and hour. For each day, solar geometries and extraterrestrial radiation at 10-min intervals are obtained; (b) Sea-level pressure in Hong Kong obtained from mean sea-level pressure observations by HKO [33]; (c) Cloudiness obtained from measurements from HKO; and (d) Monthly Linke turbidity factor in Hong Kong are obtained by Li & Lam [34]. Monthly averages of the Linke turbidity factors are used in this study. Table 1 shows the details of these input datasets. The monthly variation of Linke turbidity factors is shown in Fig. A1.

2.2. Urban canyon geometry calculation using GSV images and solar path

In this section, we introduce the use of GSV images to calculate the view factors of street canyons and solar paths in high-density urban areas of Hong Kong. The workflow procedure is shown in Fig. 3 with an example of a typical high-density street canyon. Based on our previous study [12], extractions of sky, vegetation (tree, grass, flora, and palm), and building (building, edifice, house, bridge and span) are implemented using the scene parsing method in a deep-learning framework [37] [38], as shown in Fig. 3 (a). We then project the panorama images from cylindrical to azimuthal projection to generate the fisheye images, as shown in Fig. 3 (b) and (c).

The position of the sun at a fixed observation point can be determined by specifying two angles: (1) solar zenith angle (φ, $0^\circ \sim 90^\circ$), which is defined as the angle between a vertical line and the incident solar ray; and (2) solar azimuth angle (ψ, $0^\circ \sim 360^\circ$), which is defined as the angle between the horizontal projection of the incident solar ray and the North in a clockwise direction (North is 0°). According to the SOLPOS algorithm [32], these two solar angles can be calculated based on date and time and the longitude and latitude of the observation point in a street canyon. The results of the calculated sun paths are shown as yellow dotted lines in Fig. 3 (b) and (c) for two days in different seasons, i.e., summer (August 1st, 2013) and winter (January 1st, 2013).

2.3. Calculation of total solar irradiance of street canyons

2.3.1. Physical basis of street-level solar irradiance

There are three key components in the solar radiation incident on a surface at street-level in a high-density environment as shown in Fig. 4: the direct radiation, the radiation diffused by atmospheric molecules, aerosols or clouds, and radiation reflected from buildings and ground [1] [39], [40]. As shown as beam **A,** the direct radiation is rays that come to the bottom of the street canyon in a straight line from the direction of the sun. Diffuse irradiance is the amount of radiation received by the bottom of the street canyon that has been scattered by atmospheric molecules shown as **B1**, particles shown as **B2**, and clouds shown as **B3** in the atmosphere and potentially comes from all directions. The reflected radiation is the sunlight that has been reflected off of non-atmospheric surfaces such as the ground (shown as **C1**) and buildings (shown as **C2**). Multiple scatterings and reflections by urban materials and atmosphere within the urban street canyons are not shown here. As indicated in Fig. 4, three key factors influence the street-level solar irradiance in a high-density environment:

(1) Solar geometries including solar zenith angle (SZA) and solar azimuth angle (SAA). In Hong Kong (22°17′7.87″N, 114°9′27.68″E), the SZA at local noon time changes from 45.5° in the winter and 3.5° in the summer. The solar geometries determine the associated solar irradiance on a horizon surface due to seasonal variation;
(2) Atmosphere conditions including cloudiness, local atmospheric pressure, and Linke turbidity factor. Clouds reflect and scatter solar radiation. The local atmospheric pressure and Linke turbidity factors characterize the reduction of solar radiation by absorption and scattering in the atmosphere. Turbidity index is used to quantify the clarity of the atmosphere. The Linke turbidity factor used in this study is defined as the equivalent number of standard atmospheres (dry and clean) that would have the same attenuation strength produced by the real atmosphere to attenuate extraterrestrial radiation. The factor typically ranges from 1 to 10. As shown in Li and Lam [34], the factor in Hong Kong is found to be below 5.5 for over half of the cloudless days, which indicates that on these days the clear sky conditions in Hong Kong can be defined as between turbid and clear.
(3) Street canyon geometry, including street orientation and SVF. The SVF is the fraction of sky in the upper hemisphere of a street canyon. A combination of SVF, solar path, and shading mask geometry of the street canyon determines the total incoming solar radiation that reaches the bottom of a street canyon. The orientation of a street canyon affects the timing of exposure to direct sunlight, particularly in a high-density environment with high H/W ratio. In a North-South street canyon, the street surface will be exposed to direct sunlight near mid-day but shaded in other times. However, in an East-West street canyon, it is more likely to be exposed all day from the morning to the afternoon in low latitude cities like Hong Kong [41]. Therefore, the horizon obstructions of street canyons, including buildings and trees, should be described when calculating the solar irradiance at street level.

We assume that the effect of reflections by buildings and ground can be neglected since their effect has a smaller order of magnitude with respect to the beam irradiance in clear sky conditions. In cloudy conditions, such an assumption is not always true since the radiation reflected by urban materials, such as building or ground surfaces, may become a significant part of the total irradiance. As discussed in Section 4.2, the impact of these reflections maybe comparable to diffused radiation from the atmosphere. This impact needs further investigations using complex 3-D radiative transfer simulations, which, however, are not within the scope of this article. Please refer to Section 4.2 for further

Table 1
Description of data used in this study.

	Data Source	Temporal Resolution	Description
(a) Extraterrestrial radiation	National renewable energy laboratory	10 min	Calculated using SOLPOS [32] given information of location and time
(b) Sea-level pressure	HKO	1 min	Measured at King's Park Meteorological Station by HKO [33] [35],
(c) Cloudiness	HKO	Hourly	Reported in octas hourly by trained observers at the HKO Headquarters [36]
(d) Linke turbidity factor	Li and Lam [34]	Monthly	Averaged from three different estimates. See Fig. A1 for details.

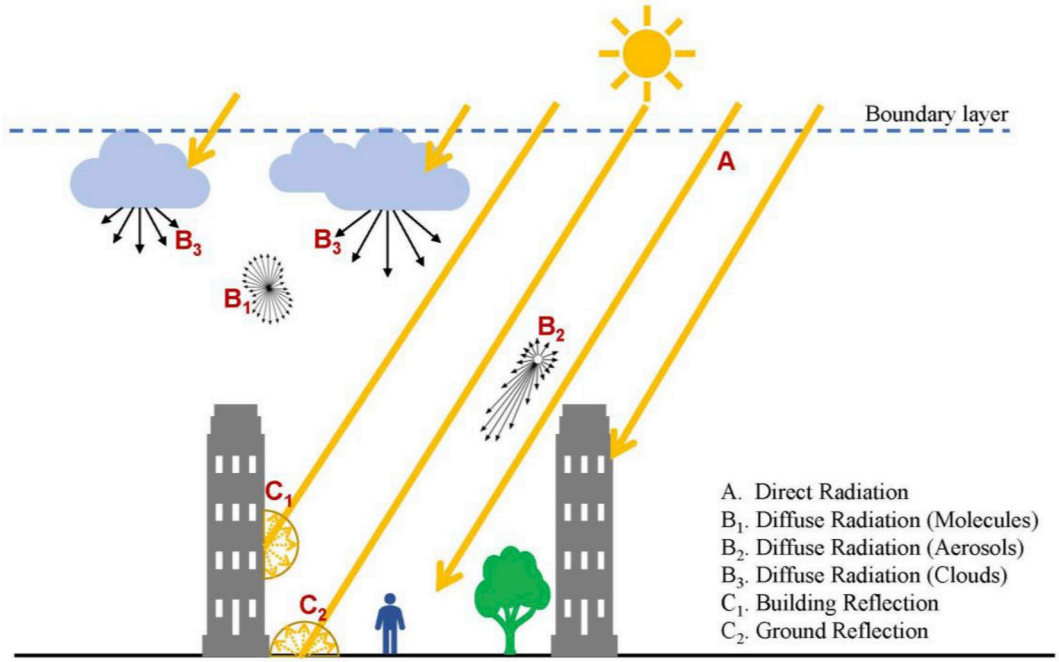

Fig. 4. Physical basis of incident solar radiation at street level in a high-density environment. As indicated, the street-level solar radiation incident on a surface includes direct and diffuse components from atmospheric molecules (Rayleigh scattering) and aerosols (Mie scattering), and clouds [42] [43], and the reflected radiation from buildings and ground. The radiation can be blocked by obstructions, such as buildings and trees, along the light path. The transmission of sunlight is subject to atmospheric absorptions which can be estimated by surface atmospheric pressure and atmospheric Linke turbidity factors.

discussions on the reflected radiation in a street canyon and its impact.

2.3.2. Calculation of street-level solar irradiance

For practicality, the direct and diffuse components of solar radiation reaching an urban street canyon can be separately approximated to be fractions of those measured in open space under an unobstructed view of the sky. As shown in the comparison of our calculations with field measurements in Section 3.1, the contribution from the reflection is actually very small compared to the daily solar irradiation.

As shown in the RayMan model [40] [44], the incoming solar radiation at the upper hemisphere of a street canyon includes the direct and the diffuse components, as shown in Eq. (1). The effect of street canyon geometries on these two components can be considered independently. For cloudless skies, direct irradiance in the street canyon depends on whether the solar radiation is blocked by buildings or trees, while diffuse irradiance is approximately proportional to the SVF.

$$G_{street} = I_{street} + D_{street} \tag{1}$$

in which the direct irradiance is given by,

$$I_{street} = I_{open} \times f \tag{2}$$

where I_{open} is the free-horizon direct irradiance and f is a binary indicator of the existence of solar ray path obstructions; f equals zero if the ray path is masked by an obstacle (such as buildings or trees), otherwise f equals one. These obstacles can be extracted using GSV images. The diffuse irradiance is given by,

$$D_{street} = D_{iso\_open} \times \Psi_{sky} + D_{aniso\_open} \times f + D_{cloud\_open} \times \Psi_{sky} \tag{3}$$

where D_{iso_open} is the isotropic diffuse radiation on a horizontal surface in a free horizon; D_{aniso_open} is the anisotropic diffuse radiation on a horizontal surface in a free horizon, which tends to concentrate in the vicinity of the sun and is discriminated depending on whether the sun is directly visible; D_{cloud_open} is the diffuse radiation on a horizontal surface in a free horizon due to clouds; Ψ_{sky} is the street sky view factor, and f is the binary indicator of obstacles. Ψ_{sky} and f can be estimated using GSV images.

2.3.2.1. Clear-sky street-level solar irradiance. The value of clear-sky solar irradiance primarily depends on the morphologies and orientations of a street canyon, and, therefore, has direct implications on urban design at street level. Based on calculations described in Jendritzky [45] and Matzarakis et al. [40], the direct irradiance I_{open} on a horizontal surface in a free horizon with no obstructions can be calculated by:

$$I_{open} = E_0 \times \cos\varphi \times \exp\left(-T_L \times \delta_{r_0} \times \frac{p}{p_0} \times m_{r_0}\right) \tag{4}$$

where E_0 is the extraterrestrial radiation; T_L is the Linke turbidity factor; δ_{r_0} is the vertical optical thickness of the standard atmosphere and m_{r_0} is the relative optical air mass, which considers the extended optical path through the atmosphere with respect to vertical incidence. The relative optical air mass is calculated [46] by:

$$m_{r_0} = 1/[\sin\gamma + 0.50572 \times (\gamma + 6.07995°)^{-1.6364}] \tag{5}$$

where the solar altitude angle $\gamma = 90° - \varphi$. The optical thickness can be calculated [47] by

$$\delta_{r_0} = 1/0.9 m_{r_0} + 9.4 \tag{6}$$

for zenith angle $\varphi < 85°$, i.e. $\gamma > 5°$.

According to the calculations as described in Valko [48] and Matzarakis et al. [40], the calculations of D_{iso_open}, D_{aniso_open}, and D_{cloud_open}

are shown below. N is cloudiness in the unit of octas. Under the cloudless assumption for calculating clear-sky solar irradiance, N = 0.

$$D_{iso\_open} = (G_0 - I) \times (1 - \tau) \times (1 - N/8) \quad (7)$$

$$D_{aniso\_open} = (G_0 - I) \times \tau \times (1 - N/8) \quad (8)$$

$$D_{cloud\_open} = 0.28 \times G_0 \times N/8 \quad (9)$$

where $\tau = I/(E_0 \cos\varphi)$ is the transmittance of the direct solar radiation. The global irradiance G_0 for undisturbed conditions (free horizon and no clouds) can be estimated [45] as follows:

$$G_0 = 0.84 \times E_0 \times \cos\varphi \times \exp\left(-0.027 \times \frac{p}{p_0} \times T_L / \cos\varphi\right) \quad (10)$$

The variables in Eq. (10) have the same meaning as Eq. (4), with the solar radiation flux density E_0 (W/m^2), the zenith angle φ (°) of the sun, the local atmospheric pressure p (hPa) relative to the normal pressure p_0 = 1,013 hPa at sea level, and the Linke turbidity factor T_L in Hong Kong [34]. As an example, Fig. 3 illustrates the calculation results of solar hours and clear-sky solar irradiation in a street canyon. However, for applications in urban areas, it is necessary to account for cloudiness, as described by the all-sky street-level solar irradiance.

2.3.2.2. All-sky street-level solar irradiance. In this study, the all-sky solar irradiance measurements without horizontal obstructions in KP from HKO are used as inputs in Eqs. (2) and (3) to calculate the all-sky street-level solar irradiance. Our use of solar radiation in KP for the whole study area is investigated in the discussion section in which we

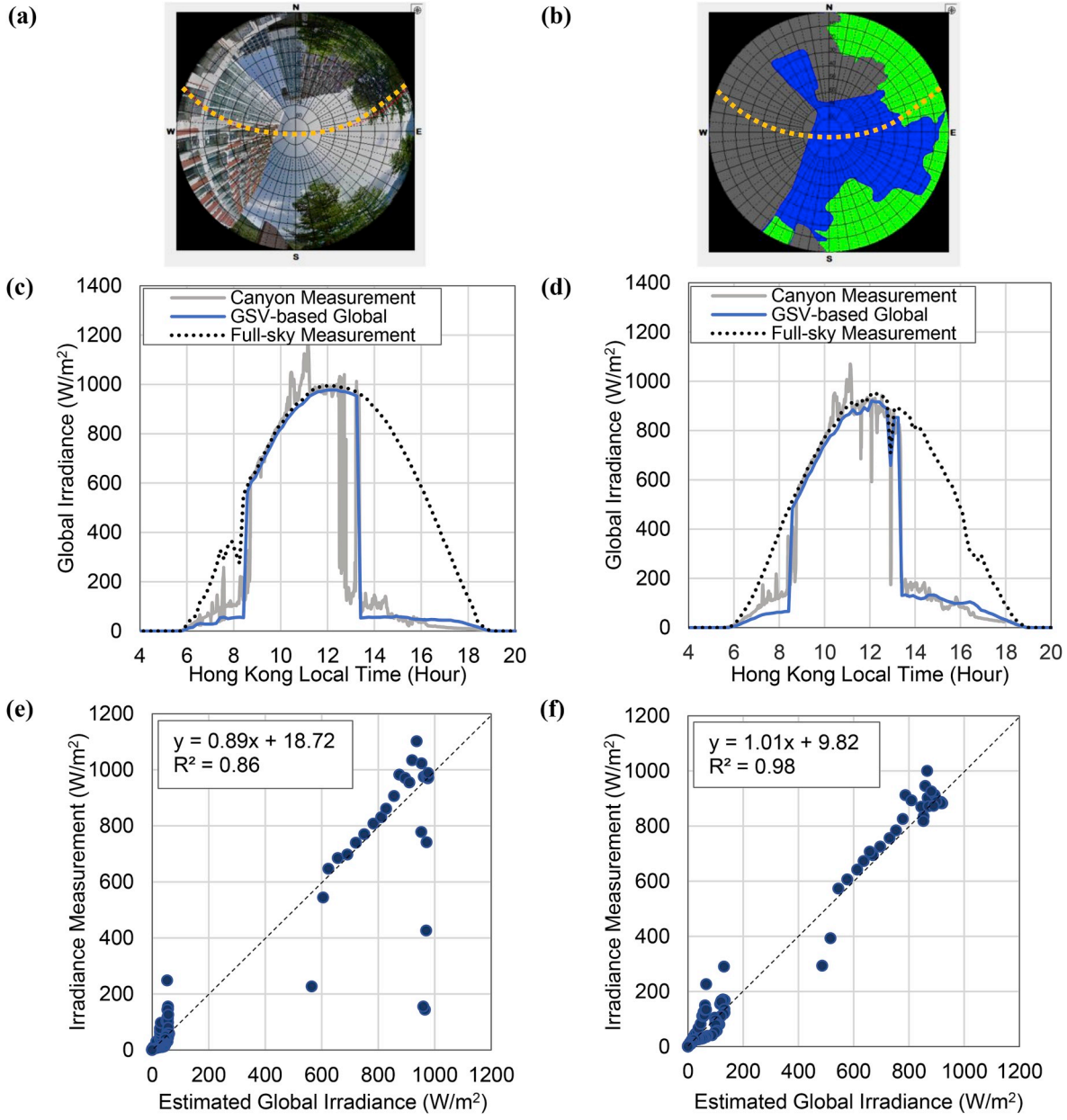

Fig. 5. Comparison of measured and GSV-based estimated global irradiance in the street canyon measurement site located in the campus of The Chinese University of Hong Kong. **(a)** Fisheye image of the street canyon; **(b)** Sky, buildings, and trees features of the street canyon; Comparision of measured and GSV-based estimated global irradiance between 05:00 h and 20:00 h for 22 May 2018 in **(c)** and 23 May 2018 in **(d)**; Scatter plots between GSV-based estimated and field measured global irradiance from 5:00 h to 20:00 h for 22 May 2018 in **(e)** and 23 May 2018 in **(f)**.

found that the free-horizon solar radiation in Hong Kong can be assumed to be homogeneous since the difference between KP (urban site) and KSC (rural site) is relatively small.

The direct irradiance measurement is the I_{open} in Eq. (2). To decompose the diffuse radiation measurements to get the D_{iso_open}, D_{aniso_open}, and D_{cloud_open} in Eq. (3), we calculate these three components using Eqs. (7)–(9) and cloudiness measurements from HKO. Calculations of these components are then scaled to fit the diffuse radiation measurements assuming the fractions from the calculations are relatively accurate. Eventually, the all-sky solar irradiance of street canyons can be calculated using Eqs. (1)–(3). The results of all-sky global irradiation of street canyons and its direct and diffuse components are shown in Section 3.2 and Section 3.3, respectively.

2.4. Accuracy assessment of GSV-based solar irradiance estimation method

To evaluate the accuracy of the developed GSV-based street-level solar irradiance estimation method, two ways of verifications are implemented: (1) street canyon verification using field measurements by LI-200R Pyranometer in a high-density environment; (2) free-horizon verification using HKO measurements of direct and diffuse radiation at KP Meteorological Station in Kowloon [35] and KSC Solar Station in Sai Kung [49].

Field measurements were conducted in May 2018 to obtain the solar irradiance of street canyons in a high-density high-rise street environment. The measurement site is located in the campus of Chinese University of Hong Kong (CUHK), as shown in Fig. 2 (b). For the

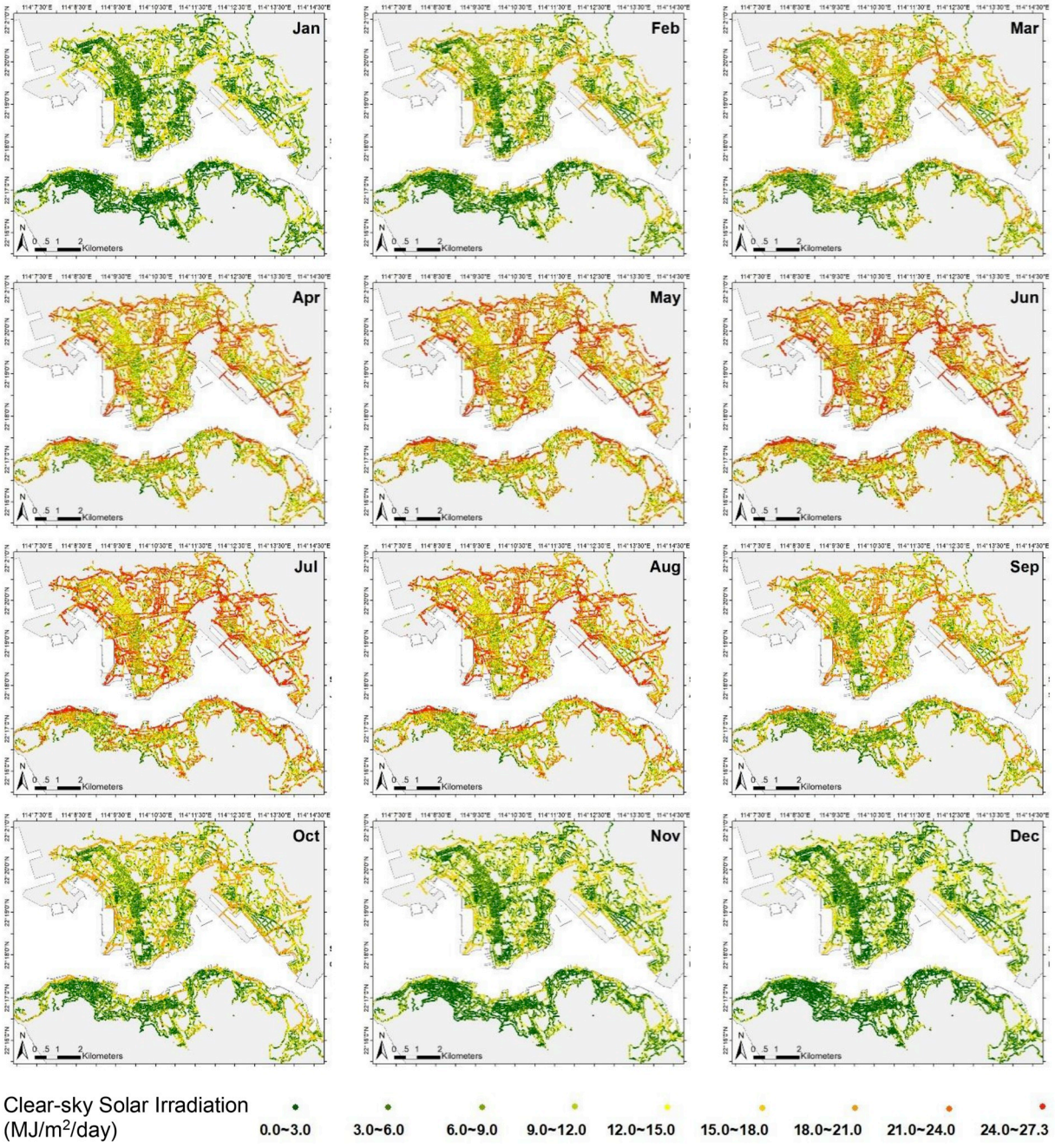

Fig. 6. Monthly mean of daily clear-sky solar irradiation (MJ/m^2/day) in street canyons averaged over six years from 2009 to 2014 in the high-density urban areas of Hong Kong. Calculation of the clear-sky solar irradiation is introduced in Section 2.3.2.

purpose of model validation, field measurements were conducted between 05:00 and 20:00 Hong Kong local time on two clear days, May 22 and May 23, 2018. The atmospheric conditions are described in Appendix B. A LI-200R Pyranometer measured global solar irradiance, i.e. the combination of direct and diffuse solar radiation in the 400–1100 nm range [50]. Table B1 summarizes the atmospheric conditions during field measurement days. The results are shown in Section 3.1.

In addition, HKO measurements of diffuse irradiance are made by a pyranometer that is shaded from the sun, while direct solar irradiance is measured by a pyrheliometer mounted on a sun tracker that ensures that it continuously points directly at the sun [49]. The direct solar irradiance is converted to that over a horizontal surface by multiplying the cosine of solar zenith angle. A real-time measurement can be seen in Ref. [51]. In this study, HKO measurements are first used to verify the calculated clear-sky solar irradiance in free horizon; second, the solar irradiance measurements in KP is used as top-of-roof solar irradiance to calculate the all-sky street-level solar irradiation given that it is effectively located in the center of our study area (Section 3.1); and finally, the difference between KP and KSC is used to characterize the spatial heterogeneity of incoming solar radiation over this region (Section 4.1).

3. Results

3.1. Verification of street-level solar irradiance estimates

In this section, the developed GSV-based solar irradiance estimation method is evaluated using field measurements in a high-density street canyon. Further verification against HKO measurements under free-horizon view is described in Appendix C.

Calculation of all-sky street-level solar irradiance developed in this study based on GSV images and HKO measurements is verified using field measurements in a high-density urban street canyon. Fig. 5 presents the measured and simulated global radiation for two consecutive days, 22-23 May 2018. Fig. 5 (a) shows the fisheye image of the street canyon with the corresponding solar path over a day. The panorama classification is shown in Fig. 5 (b) for the sky, tree, and building, of which the values of SVF, TVF, and BVF are 0.47, 0.13, and 0.40, respectively. The sun path is obstructed by trees in the eastern section of the street canyon in the morning before ~8:00 h and by the buildings in the western section of the street canyon in the afternoon after 13:00 h. Between 8:00 h and 13:00 h, when the sky is open, we can see the calculated global irradiance fits very well with the street canyon field measures and the free-horizon HKO data, as shown in Fig. 5 (c) and (d). The small spikes in field measurements during 10:30–11:00 h is due to the specular reflectance from the building windows, which is hard to capture in the calculation. The sharp drawdown at around 13:00 h is very likely due to clouds. During 6:30–8:30 h, the field measurement data is slightly higher than the GSV-based estimated radiation. This is probably because the sunlight is not totally blocked by the trees and there is still some transmissivity of solar radiation through the tree crowns. When the sun path is obstructed, the solar radiation decreases dramatically relative to free-horizon radiation and is reduced to be only from diffuse radiation. We can see the calculations well capture the temporal pattern of the diffuse radiation. The differences between calculated and measured global irradiance range from −20 to +20 W/m^2 during sunshine hours. These differences can be partly explained by the effect of reflected radiation within the street canyon. The differences increase to more than 20 W/m^2 in the afternoon when there are clouds. Fig. 5 (e) and (f) shows that the coefficients of determination (R^2) of estimated and measured global irradiance are 0.86 and 0.98, respectively. The outlier points off the diagonal line are due to clouds or specular reflectance. From these results, we can conclude that the general pattern of the solar irradiance in a street canyon can be predicted by the developed GSV-based model.

3.2. Spatiotemporal pattern of solar irradiation of street canyons

In this section, street-level solar radiation is calculated using the GSV-based method under two conditions: (1) clear-sky solar irradiation under ideal clear-sky assumptions to investigate the effects of street morphologies and geometries; and (2) all-sky solar irradiation based on HKO measurements to investigate the impact of clouds. Clear-sky street-level solar irradiation is the solar radiation in street canyons under clear day (no cloud) assumptions. Its spatial and temporal patterns are therefore dominantly affected by solar geometries, street canyon geometries (street orientation and aspect ratio), and morphologies (sky opening and obstructions by buildings and trees). Fig. 6 shows the monthly mean of daily clear-sky solar irradiation averaged over six years from 2009 to 2014 in the high-density urban areas of

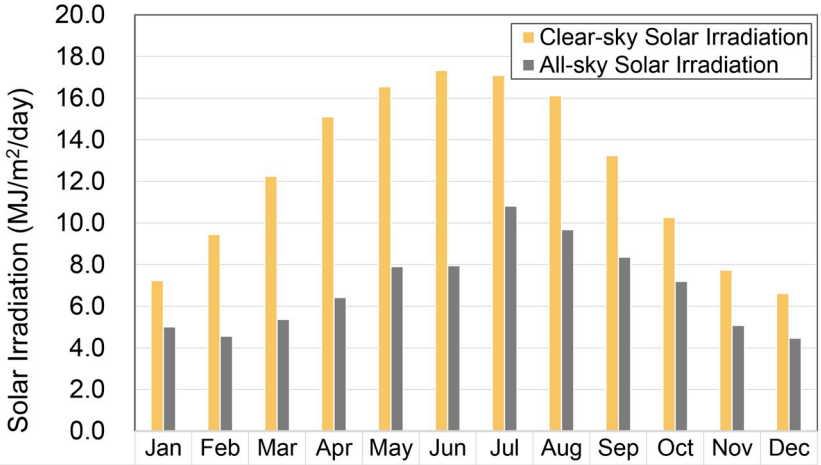

	Jan	Feb	Mar	Apr	May	Jun	Jul	Aug	Sep	Oct	Nov	Dec
Clear-sky Solar Irradiation	7.2	9.5	12.2	15.1	16.5	17.3	17.1	16.1	13.2	10.3	7.7	6.6
All-sky Solar Irradiation	5.0	4.6	5.4	6.4	7.9	8.0	10.8	9.7	8.4	7.2	5.1	4.5

Fig. 7. Comparative analysis of monthly mean of the calculated daily clear-sky and all-sky solar irradiation (MJ/m^2/day) based on 25,654 street canyon samples using Google Street View images in the high-density urban area of Hong Kong.

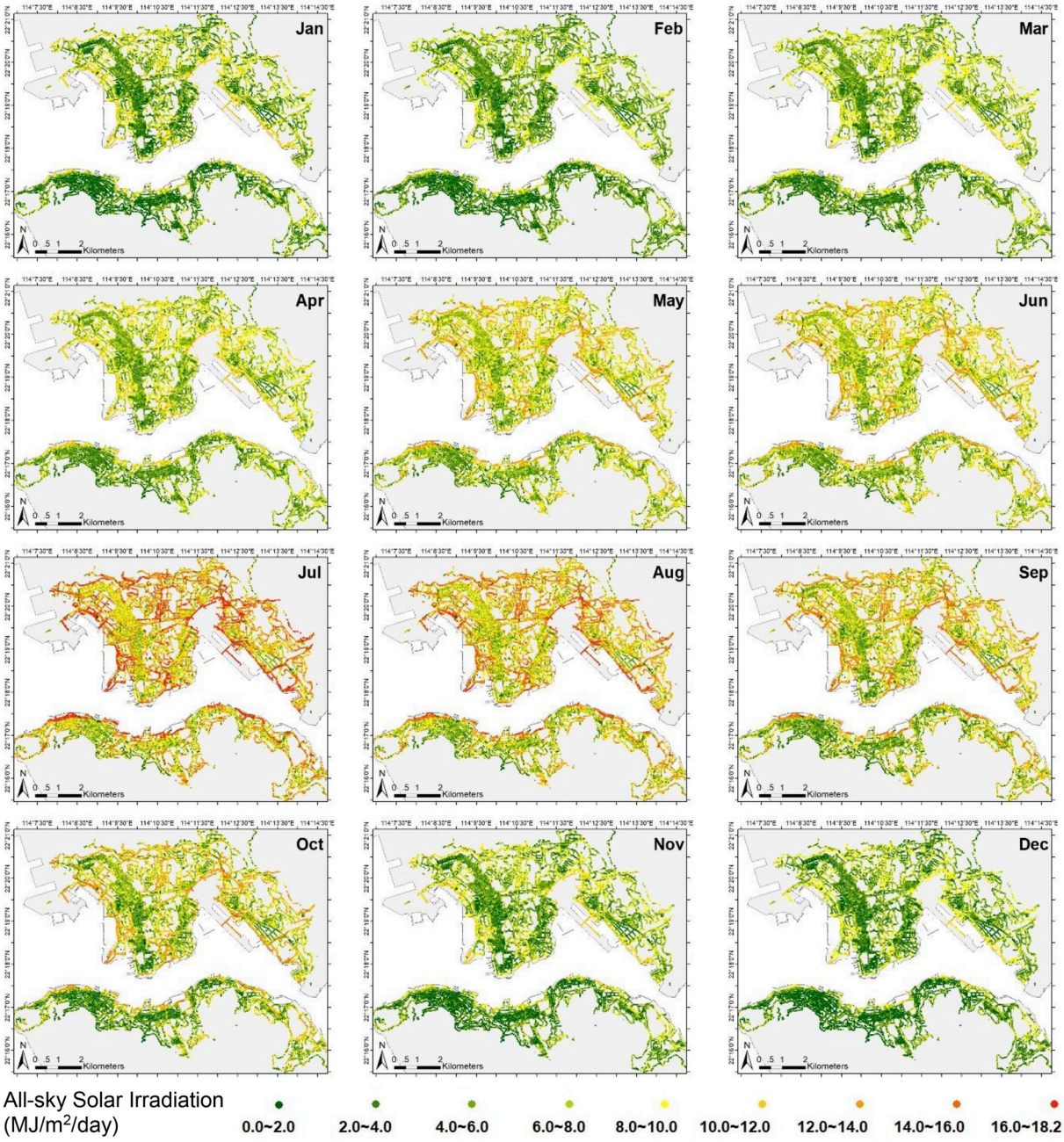

Fig. 8. Same as Fig. 6 but for all-sky street-level solar irradiation. **These** monthly means of daily all-sky solar irradiation (MJ/m^2/day) in street canyons are averaged over six years from 2009 to 2014 in the high-density urban areas of Hong Kong. The detail of the calculation is introduced in Section 2.3.2.

Hong Kong. A strong seasonal variation with high values in the summer and low values in the winter can be observed. This temporal pattern mainly follows the seasonal variation of incident solar zenith angle. As shown in Fig. 7, the lowest monthly averaged value is ~6.6 MJ/m^2/day in December and the highest value is ~17.2 MJ/m^2/day in July. Higher daily solar irradiation of street canyons (> 20.0 MJ/m^2/day) occurred during the summer season is mainly distributed in open space areas (SVFs are around 0.7–1.0) or street canyons with West-East orientation (SVFs are around 0.3–0.6). Lower solar irradiation of street canyons (< 10.0 MJ/m^2) during most of the winter season is mainly distributed in high building density areas (BVFs are around 0.7–0.8) or high tree coverage areas (TVFs are around 0.6–0.8). From Fig. 6, two distinct spatial features can be seen: (1) the spatial variability is closely related to building densities as shown in Fig. 2 (c) in Gong et al. (2018) in which much lower solar radiation is received in streets surrounding by high-density buildings. A similar pattern of spatial variation can also be seen in GSV-based SVF estimates as shown in Fig. 2 (c); (2) streets with West-East orientation receive higher solar radiation than surrounding regions in summer when SZA is small and the street is exposed to solar radiation for the whole day. In winter, the SZA is large and therefore most of the direct solar irradiation is obstructed by buildings. Further analysis of street-level irradiation with different street canyon

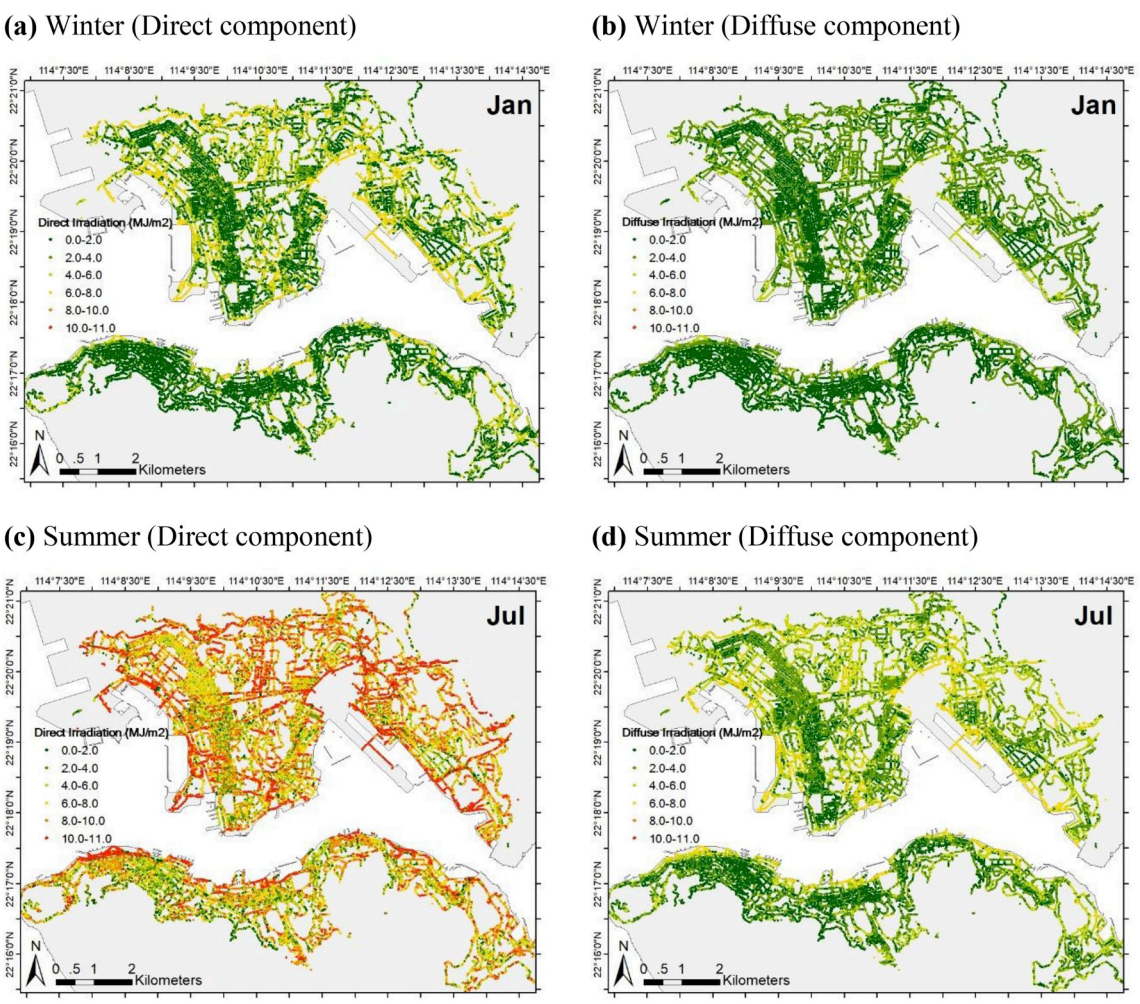

Fig. 9. (a) Daily direct irradiation (MJ/m^2/day) of street canyons in high-density urban areas of Hong Kong in January averaged for six years (2009–2014); **(b)** Daily diffuse irradiation (MJ/m^2/day) of street canyons in January averaged for six years (2009–2014); **(c)** the same as (a) but for July, an example of July in summer; **(d)** The same as (b) but for July. These are all-sky street-level solar irradiation estimates based on GSV images and HKO measurements as described in Section 2.3.2.

morphologies is presented in the following Section 3.4.

Fig. 8 shows the corresponding monthly mean all-sky solar irradiation of street canyons calculated using GSV images and realistic HKO measurements as described in Section 2.3.2. As shown in Fig. 7, when a realistic cloud effect is considered in the calculation, the solar irradiation value drops significantly, especially from February to June the values are less than half of the corresponding clear-sky solar irradiation. This is because clouds cover 80% of the sky on average from February to June in Hong Kong, according to the long-term cloud data from HKO [52]. During the summer season, the dominant weather condition is cloudy, especially in the early afternoon [53]. Cloudy conditions, with cloud amount reaching 6 octas or above, occurred during about 70% of the summer, mostly between 12:00 h and 15:00 h in the afternoon [36]. From Fig. 7, we can see that the lowest and highest monthly mean solar irradiation are 4.5 MJ/m^2 in December and 10.8 MJ/m^2 in July.

The spatial patterns of the all-sky solar irradiation shown in Fig. 8 are similar to those in the clear-sky solar irradiation as shown in Fig. 6. Similarly, the street geometries and morphologies have dominant imprints on the spatial pattern of the all-sky solar irradiation. To quantitatively compare the street-level solar irradiation in extreme high-rise and low-rise street canyons, we calculate the means with SVF≥0.7 and SVF≤0.3, respectively. We found that in summer, the irradiation in an extreme low-rise region (16.1 MJ/m^2/day) is on average about three times higher than that in extreme high-rise region (5.6 MJ/m^2/day). In winter, the low-rise and high-rise irradiations are 9.1 MJ/m^2/day and 1.8 MJ/m^2/day on average, respectively, differing by a factor of five.

3.3. Contributions from direct and diffuse components

For each specific street canyon, the horizon obstructions (e.g. buildings and trees) will exert independent effects on the direct and diffuse radiation. When the sun is masked by an obstacle, such as buildings or trees, the direct radiation in Eq. (2) and the anisotropic diffuse radiation in Eq. (3) will be totally blocked. The remaining portion of solar diffuse radiation, i.e. the isotropic diffuse radiation, enters the street through the sky opening. For cloudless skies, direct irradiance in street canyons is determined by whether the solar disk is obstructed or not, while diffuse radiation in street canyons is proportional to the amount of sky opening, i.e. SVF. For this reason, a detailed study of the spatial patterns of direct and diffuse irradiation provides further clues on how street morphologies affect the two components of street-level solar irradiation. To calculate their contributions to the

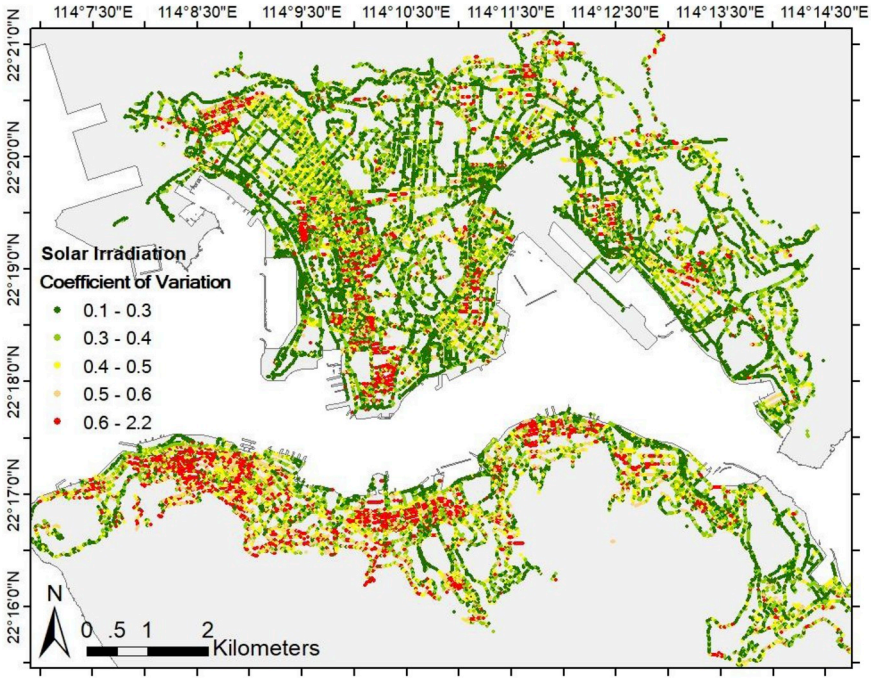

Fig. 10. Coefficient of variation, defined as the ratio of standard deviation to mean, of daily solar irradiation calculated using 2,190 days of all-sky solar irradiation data over the six years from 2009 to 2014.

total irradiation, it is first necessary to split the global radiation into the direct and diffuse components, as shown in Eq. (1).

Fig. 9 illustrates the direct and diffuse irradiation separately for winter (January) and summer (July) averaged over six years from 2009 to 2014. For the direct irradiation, shown in Fig. 9 (a) and (c) for winter and summer, respectively, the spatial patterns are similar but the value in summer is about two times higher than that in winter, especial in street canyons with East-West orientation. This is because the SZA is summer is much smaller than that in winter. Moreover, there is less obstruction by buildings or trees in summer when SZA is smaller. For the diffuse irradiation, there are large differences in spatial patterns in the two seasons. In summer days, as expected, the areas have higher diffuse irradiation than that in winter days, as shown in Fig. 9 (b) and (d), because the anisotropic diffuse component in summer, when the sun path is less obstructed, is higher compared to that in winter. For the direct and diffuse irradiations in winter as shown in Fig. 9 (a) and (b), the value in the high-density regions is very low. The direct component is higher than the diffuse component in the open areas with high SVF. However, the street orientation has a relatively small effect on received solar radiation in winter because of a relatively short exposure time of direct solar irradiation due to sunlight obstructions.

3.4. Effect of street canyon geometry on solar irradiation

An investigation of the variation of street-level solar irradiation between different seasons is directly linked to the street geometry and morphologies and therefore helps identify regions with solar radiation over-exposure in summer but under-exposure in winter. Fig. 10 shows the coefficient of variation, defined as the ratio of standard deviation to mean, of daily solar irradiation calculated using 2,190 days of all-sky solar irradiation data over the six years from 2009 to 2014. We can see that high variability is mainly located in high-density street canyons, especially in streets with West-East orientation, while low variability can be seen at low-density build-up areas and streets with non-W-E street orientation. This agrees with the month to month variability as shown in Fig. 8.

To further examine the dependence of solar irradiation on urban street geometries and morphologies, which are characterized by street orientation and H/W ratio, we select six different examples of street canyons, including three different types of street geometries with H/W ratios of ½, 1, and 2, respectively, and two different types of street orientations of North-South and West-East, as shown in Fig. 11. The SVF of these street canyons changes from 0.2 to 0.8, and the daily clear-sky solar irradiation changes from about 1.0 MJ/m^2/day in winter to more than 16 MJ/m^2/day in summer. Fig. 12 shows the monthly mean of the daily all-sky global, direct, and diffuse irradiation corresponding to the six types of street canyons. As expected, solar irradiation increases as SVF increases from high-rise (H/W≥2:1) to low-rise (H/W≤1:2). The important role of street orientation in the incident solar irradiation can be observed in street canyons of West-East and South-North orientations with the same aspect ratio. In general, street canyons with West-East orientation receive higher solar radiation in the summer season from March to September but lower in the winter season. This difference results from the change of solar incident zenith angle between summer and winter. When SZA is small in summer, the West-East orientation streets are exposed to solar radiation for a much longer time from morning to afternoon compared to North-South orientation street while in winter when SZA is high, most solar radiation is obstructed by buildings and trees for a West-East orientation street. However, the North-South orientation street can still get exposure to solar radiation at noon. As shown in Fig. 12 (b) and (c), this difference is obvious in total solar irradiance and direct component, but not in the diffuse component, which is nearly similar for different street orientations.

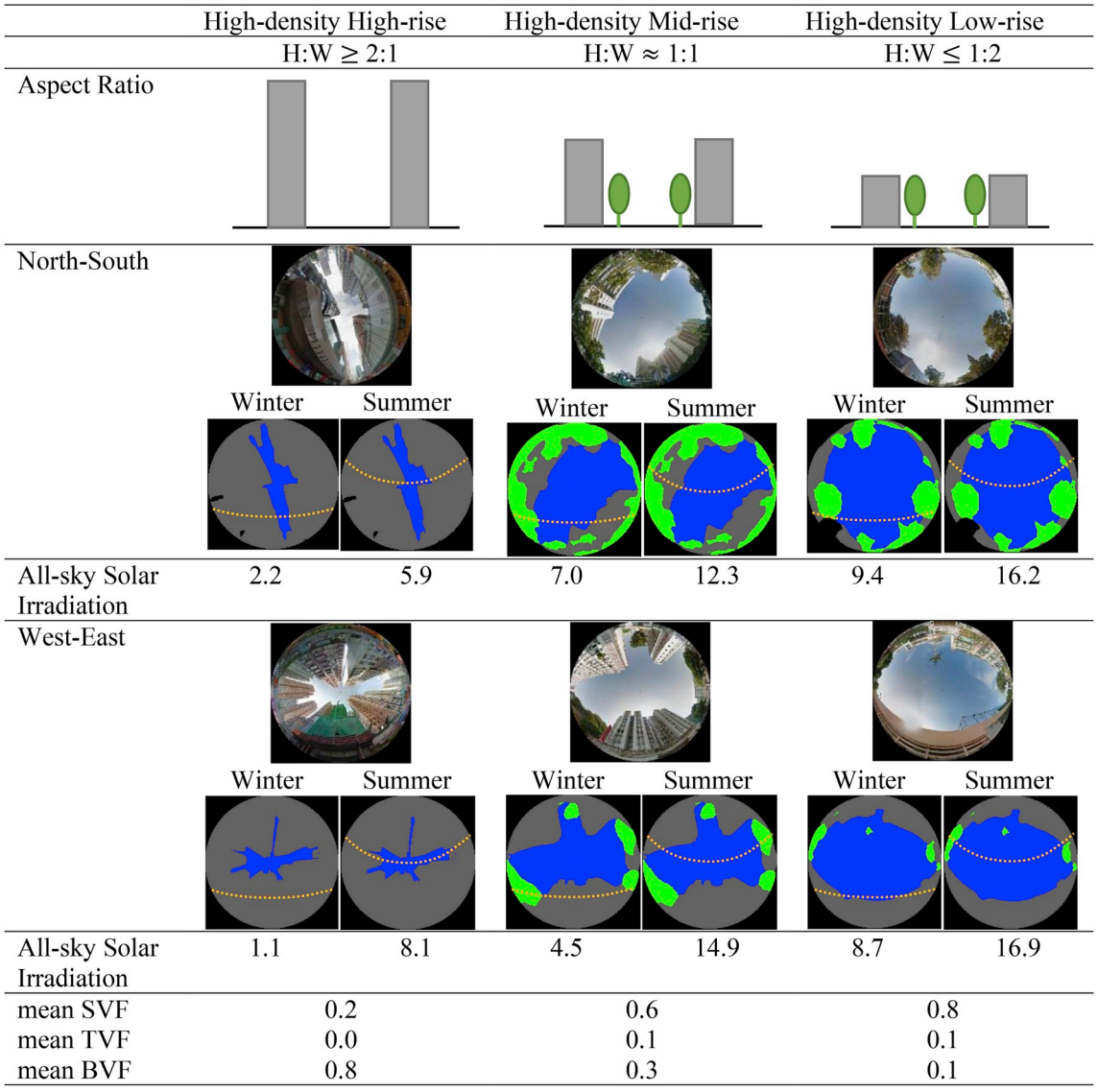

Fig. 11. Six different types of street canyons, including three different types of street geometries with H/W ratios of ½, 1, and 2, respectively, and two different types of street orientations of North-South and West-East. The daily all-sky solar irradiation (MJ/m^2/day) for summer and winter are also indicated, respectively, as well as sky view factors (SVF), tree view factors (TVF), and building view factors (BVF).

4. Discussion

4.1. Spatial inhomogeneity of solar radiation

In this study, the solar irradiance measurements in KP, which is located in the middle of the study area as shown in Fig. 2 (b), are assumed to represent the whole study area and are used in Eqs. (2) and (3) to calculate the all-sky street-level solar irradiance. Here we compare the measurements from KP and KSC sites to justify this assumption. KSC is located to the north-east of the study area (Fig. 2 (b)) and the distance between KSC and KP is about two times the width/length of the study area. The difference between the two characterizes the spatial homogeneity of incident solar radiation over this region. As shown in Fig. 13 (a), in general, the global radiation at KP agrees closely with that in KSC. KSC, a more rural setting, has a slightly higher amount of direct solar irradiation in most months than KP in a more urban environment, probably due to the stronger effect of aerosol extinction in KP. The largest difference in the summer months is about 10% in global radiation. The diffuse radiation is almost the same between KP and KSC, indicating the cloud diffusion effect is not causing bias in spatial distribution over this region. These results imply that the spatial difference in incident global solar radiation is small over the whole Hong Kong territory. A similar conclusion can be reached from Fig. 13 (b), more than 90% of the days have a difference less than 2.0 MJ/m^2/day for both direct and diffuse components at street level. Within the uniformly high-density urban study area, the difference should be even smaller, and therefore these results justify our assumptions of spatial homogeneity of incident solar radiation.

4.2. Reflected radiation in a street canyon and its impact

Multiple reflections by urban materials within the urban street

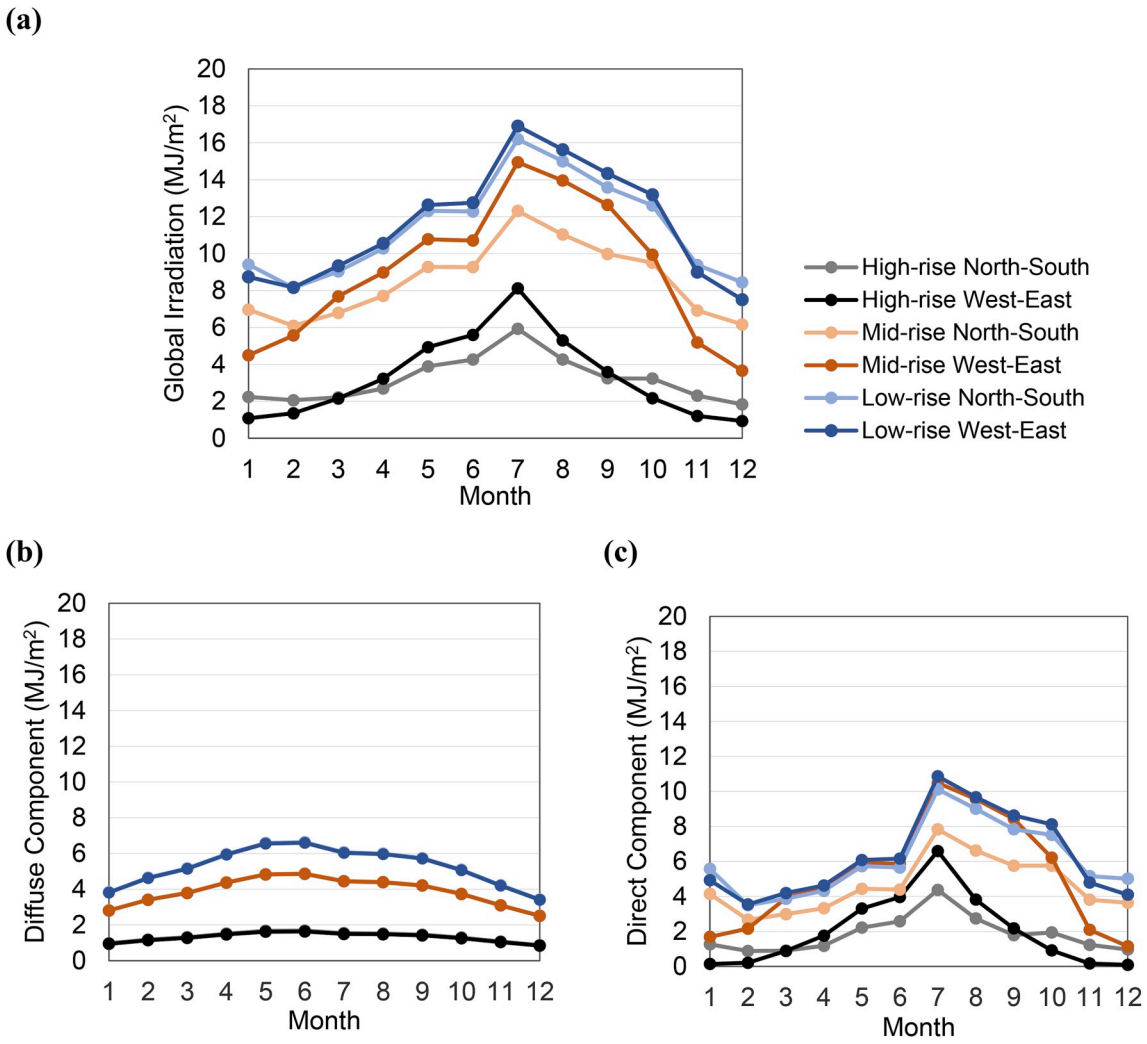

Fig. 12. Monthly mean of daily all-sky solar irradiation (MJ/m^2): **(a)** global irradiation, **(b)** diffuse irradiation and **(c)** direct irradiation for the six types of street canyons in high-density urban areas of Hong Kong averaged for six years from 2009 to 2014.

canyons are not considered by this GSV-based calculation method. The modelling of the contributions from these multiple reflections would require complex 3-D radiative transfer simulations. For applications on large spatial and temporal scales which require simple and fast calculations, the effect of these reflections is neglected. According to our verification results in Section 3.1, we can see that our calculation method well captures the direct and diffuse components in a street canyon. The reflectances by street buildings, trees and roads are relatively small. The reflectance effect may become evident in the street canyons with glass walls with high reflectance at certain SZA.

The reflected radiation by urban materials (e.g. building walls, ground, and trees) exposed to direct radiation may become important when there is no direct irradiance on the street during the day, which is common in high-density street canyons during the winter season. From our results, about 9.7% of the street canyons receive zero direct solar radiation in January and about 1.0% in July (see Fig. 14). In this case, the radiance received is only from the diffused radiation by the atmosphere and reflected radiation by the buildings. As shown in Fig. 2 of Ali-Touder & Mayer [54] using 3-D numerical model simulation, the diffuse component increases as the aspect ratio H/W increases because of the reflected radiation from the buildings. The increment of about 100 W/m^2 at maximum as H/W changes from low (0.5) to high (4.0) is comparable to the total diffuse component (approximately 150 W/m^2) for the widest geometry. This indicates that in a street canyon the reflected radiation by buildings and the diffuse component by the atmosphere may be similar in terms of magnitude. The daily diffuse irradiation from the atmosphere is about 0.60 MJ/m^2 on average in January for the street canyons without direct solar radiation. This value is relatively small when the street canyon is exposed to direct solar radiation, which, according to our estimation when the direct solar exposure time is longer than 1 h, is larger than 3.5 MJ/m^2 in January (account for 73.1% of the street canyons) and 5.1 MJ/m^2 in July (account for 96.7% of the street canyons). Since the effect of reflections may be relatively important only when there is no direct solar radiation shining on the street in a day which only happens over a limited number of street locations, we therefore expect the impact of reflected radiation by buildings to be very small on the spatiotemporal patterns of daily solar irradiation.

For future studies, GSV images may potentially be used to make a first-order estimation of the reflected radiation from buildings by constructing a correlation between diffuse irradiance and street view factors using 3-D simulations.

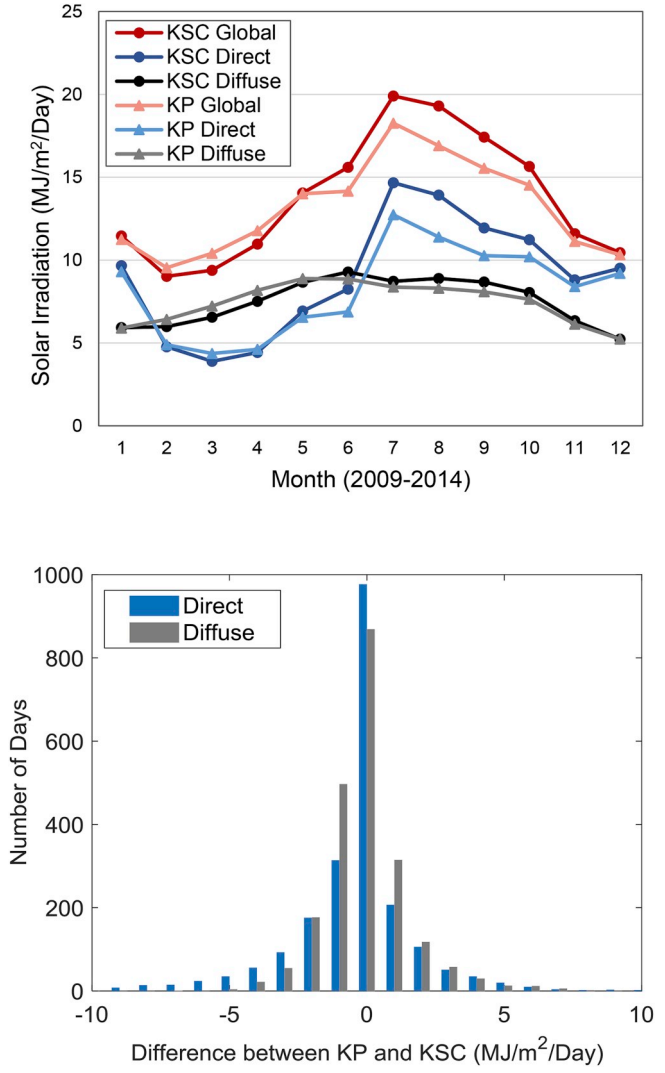

Fig. 13. (a) Comparison of monthly mean of daily solar irradiation measured at King's Park (KP) site and Kau Sai Chau (KSC) site of Hong Kong Observatory from 2009 to 2013; **(b)** The histogram of the difference between daily solar irradiation at KP and KSC.

4.3. Transmissivity of solar radiation through tree crowns

In this study, street trees are considered to be the same obstructions as buildings and the solar transmissivity of tree crowns is assumed to be zero. The uncertainty from this assumption may be small when trees leaves are dense. This is a reasonable assumption since Hong Kong is located in the subtropical monsoon region where the street trees can be nearly maintained throughout the year [55], [56]. However, it has been shown that the average transmissivity of direct solar radiation through the foliated and defoliated tree crowns ranges from 1.3 to 5.3% and from 40.2 to 51.9%, respectively [57]. In the developed GSV method, this solar transmissivity ratio of street trees can be refined to a larger value based on different tree types. In cases when building surfaces overlap with tree canopies, building 3-D model may be used to extract the masked areas of trees or building surfaces. The effects of tree transmissivity on urban environments should also be investigated in future studies. Pyranometers can be used to measure crown transmissivity of local tree species, and different vegetation layer should be given different properties such as surface albedo, emissivity and transmittance. Moreover, tree transmissivity for the same tree species with different tree-canopy characteristics (e.g. leave density and canopy size) should also be investigated.

5. Conclusions

This study focuses on (1) developing an approach for accurately calculating the street-level global, direct, and diffuse solar irradiance in high-density urban environments using publicly available GSV images; (2) quantifying the spatial and temporal patterns of street-level solar irradiation in the high-density urban areas of Hong Kong; and (3) investigating the impacts of street canyon geometries (street orientation and aspect ratio) and morphologies (sky opening and obstructions by buildings and trees) on street-level solar irradiation. Verifications of our developed method using free-horizon observatory from HKO and field measurements in a high-density street canyon show that both the clear-sky (without cloud effects) and all-sky (with cloud effects) solar irradiance of street canyons accurately capture the diurnal and seasonal cycle in high-density environments. The key points from this study are:

- A strong seasonal variation with high values in the summer and low values in the winter can be observed in both clear-sky and all-sky street-level solar irradiation.
- The spatial variability of street-level solar irradiation, both clear-sky and all-sky, is closely related to building densities in which much lower solar radiation is received in streets surrounding by high-density buildings. The global irradiation in low-rise regions is about three times that in high-rise regions in summer and about five times in winter.
- For the direct irradiation, the spatial patterns are similar but the solar irradiation in summer is about two times higher than that in winter. For the diffuse irradiation, there are large differences in spatial patterns in the two seasons. In summer, the areas with large SVF have higher diffuse radiation than that in winter.
- Street orientation has a large impact on the solar radiation received by a high-density street canyon. Street canyons with West-East orientation receive higher solar radiation in the summer and lower in winter than North-South orientation. The impact by street orientation is larger in high-rise than low-rise street canyons.

The developed method in this study to map the street-level solar radiation can be, on a global scale, applied to cities with available coverage of GSV images. This method provides a low-cost and effective streetscape mapping approach for urban studies. Clear-sky street-level solar irradiance can be derived for cities with basic meteorological measurements including atmospheric pressure while all-sky street-level solar irradiance can be further calculated if free-horizon solar irradiance is available at a local site, such as HKO measurements in Hong Kong. The resulted maps of street-level solar irradiation provide crucial datasets for studying the spatial and temporal variabilities of street-level solar irradiation and understanding the interactions between solar radiation, human health and the urban thermal balance in the high-density urban environment.

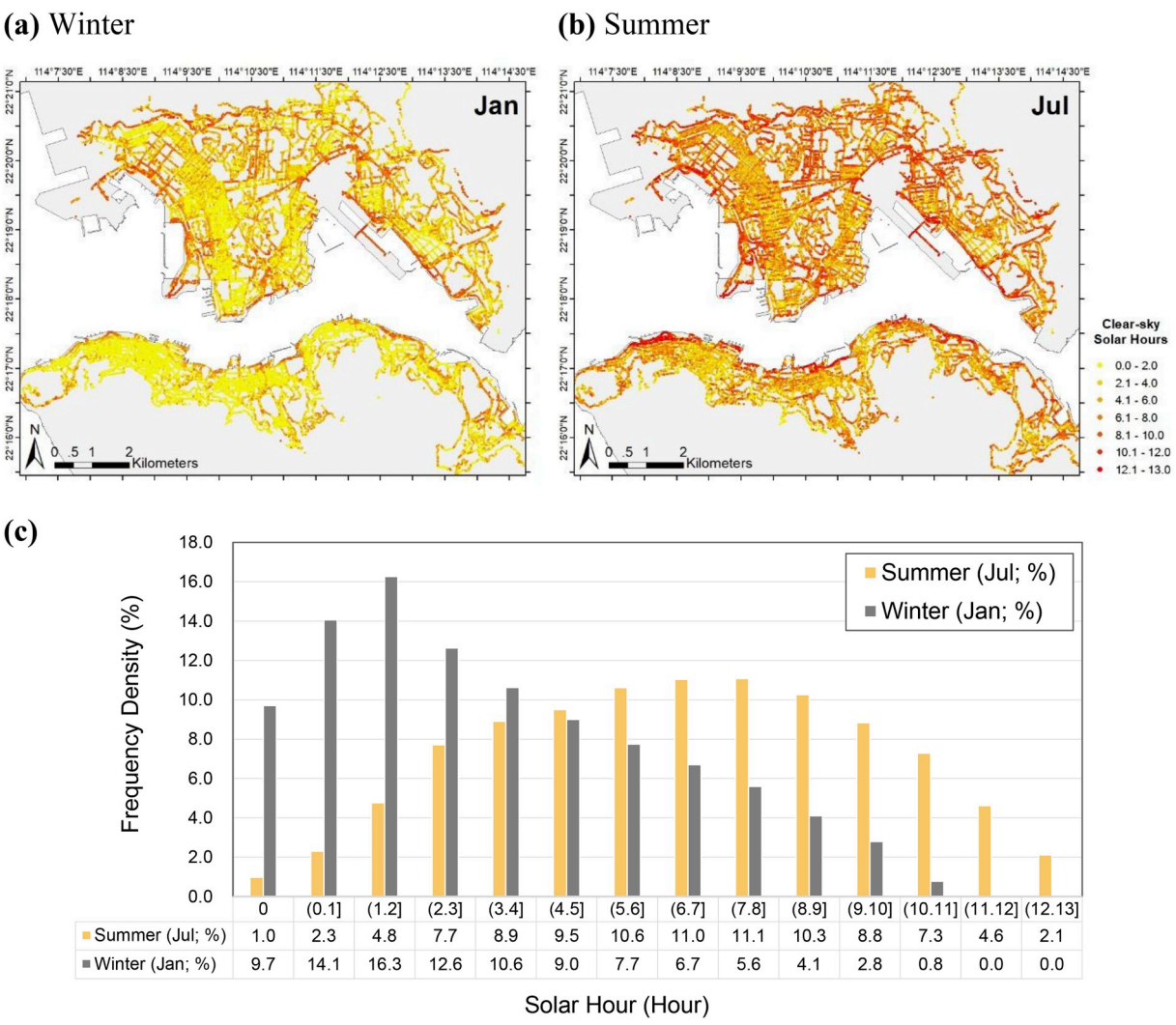

Solar Hour (Hour)	0	(0.1]	(1.2]	(2.3]	(3.4]	(4.5]	(5.6]	(6.7]	(7.8]	(8.9]	(9.10]	(10.11]	(11.12]	(12.13]
Summer (Jul; %)	1.0	2.3	4.8	7.7	8.9	9.5	10.6	11.0	11.1	10.3	8.8	7.3	4.6	2.1
Winter (Jan; %)	9.7	14.1	16.3	12.6	10.6	9.0	7.7	6.7	5.6	4.1	2.8	0.8	0.0	0.0

Fig. 14. Monthly mean of daily clear-sky solar hours in street canyons, averaged over six years from 2009 to 2014 in the high-density urban areas of Hong Kong, in the winter in **(a)** and summer in **(b)**. Comparison analysis of the frequency of solar hours in summer (July) and in winter (January) in **(c)**.

Acknowledgments

The study is supported by the Postgraduate Scholarship (PGS) and the Global Scholarship Programme for Research Excellence from The Chinese University of Hong Kong. We would like to thank Dr. Fan Zhang from Peking University for assistance in processing the Google Street View images. The authors also wish to give special thanks to the two reviewers for their valuable comments and suggestions that help to improve our research. We also thank the editors for their patient and meticulous work for our manuscript.

Appendix A. Linke turbidity factor

Fig. A.1 shows the monthly averaged Linke turbidity factors (in black) in Hong Kong. These factors are adopted from Table 2 in Li and Lam [34]. We calculated the average Linke turbidity factor from three estimates: T_{Lin}, T_{Lou}, and T_{Pin} which correspond to three different estimation methods. The T_{Vis} in Li and Lam [34] is not used because it is very different from the other three estimates.

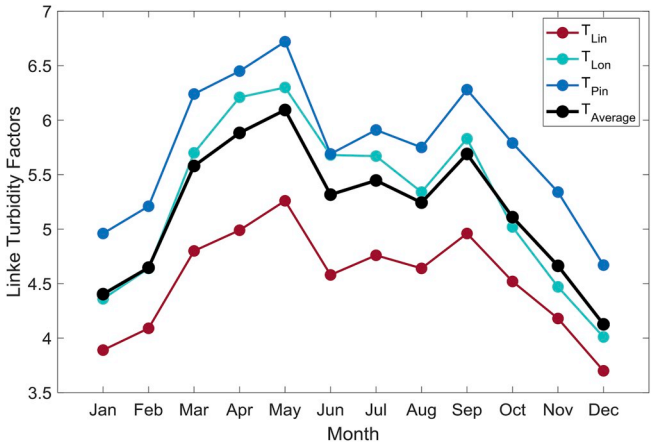

Fig. A.1. Monthly averaged Linke turbidity factors (in black) in Hong Kong. Based on Table 2 in Li and Lam [34], the Linke turbidity factor used in this study is the average value of three different estimates: T_{Lin} (in red), T_{Lou} (in green), and T_{Pin} (in blue).

Appendix B. Field measurements

Table B.1 describes the associated atmospheric conditions and site information for field measurements. The temporal sampling interval and measurement time are also indicated. Fig. B.1 shows the measured free-horizon global, direct and diffuse solar irradiance. According to Li and Lam [34], the clear-day criteria are given by: (a) The direct normal irradiance is greater than 200 W/m^2; (b) The ratio of the diffuse component to global irradiance should be less than 1/3. From the results of free-horizon solar irradiance measurements in Fig. B.1, we can see 22-23 May 2018 meet the criteria for clear days.

Table B.1
Summary of associated atmospheric conditions used in the model

Time information			**Atmospheric conditions**		
Date	Time (hour)	Interval	Highest free-horizon solar irradiance (W/m^2)	Minimum solar zenith angle (degree)	Mean sea-level pressure (hpa)
22-May-2018	05:00–22:00	15 s	997.3	4.2	1010.5
23-May-2018	05:00–22:00	15 s	963.6		1009.6
Site information			**View factor (VF)**		
Longitude	Latitude	Altitude	SVF	TVF	BVF
114°12′36.1″E	22°25′06.1″N	50.0 m	0.47	0.13	0.40

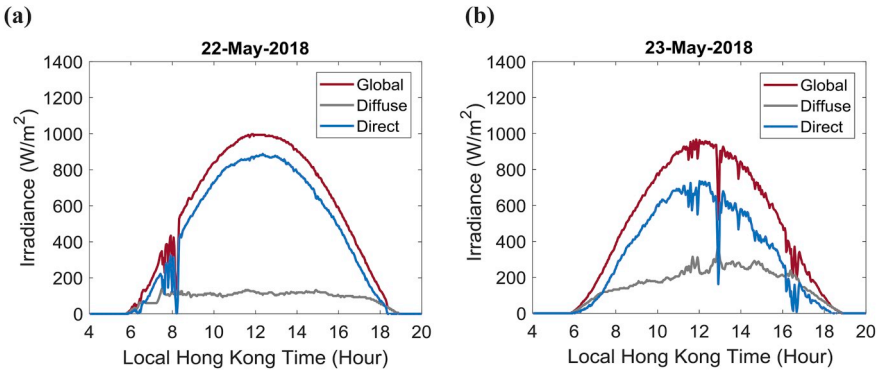

Fig. B.1. The free-horizon solar irradiance measurements by HKO for May 22, 2018 in **(a)** and May 23, 2018 in **(b)**.

Appendix C. Verification using HKO free-horizon solar irradiance measurements

Multi-year HKO solar irradiance measurements in free horizon provide an essential way to verify our proposed method for estimating street-level all-sky irradiance under all cloud conditions. The hourly mean of free-horizon solar irradiance is calculated for the King's Park site with associated atmospheric conditions, including sea-level pressure (see Fig. C.1(a)), Linke turbidity factor (see Fig. A.1), and cloudiness from HKO (see Fig. C.1(b)). The results are then compared with HKO solar irradiance measurements by investigating their difference. Given the large uncertainty from the cloud effect, the differences in direct, diffuse and global solar irradiance are plotted for three sets of different cloud coverages, as shown in Fig. C.2 and C.3. In total, 2,190 days of data from 2009 to 2014 are used. As shown in Fig. C.2, the case for clear days (octas = 0) has the best accuracy with the

highest correlation coefficient (0.99) and the smallest RMSE (46.2 W/m^2) for global irradiance. This result justifies the method described in Section 2.3.2 to calculate the clear-sky solar radiation under clear-sky assumptions. In general, for the semi-cloudy condition (octas = 1–7), the calculated solar irradiance tends to underestimate the HKO measurements, while for the overcast condition (octas = 8), the calculated solar irradiance tends to be overestimated. Results from further statistical analysis demonstrate that: (1) the overall correlation coefficient for global solar irradiance under all-sky conditions (for all octas from 0 to 8) is 0.87 and the RMSE is 138.2 W/m^2; (2) about 47.6% of the solar irradiance calculations under all cloud conditions (octas from 0 to 8) have errors smaller than 50 W/m^2. The accuracy of the calculation method under partially cloudy conditions remains to be improved, given that current parameterized models cannot account for cloud movement across the sky that may create complex patterns of reduced and enhanced radiation values.

Three examples with clear, semi-cloudy, and overcast days are shown in Fig. C.3 to investigate the diurnal variability of calculated solar irradiance under different cloudiness conditions compared with HKO measurements. The global, direct and diffuse solar irradiance are illustrated. We can see in general the calculated solar irradiance well captures the diurnal variabilities of the measured HKO solar irradiance on the clear day. However, there are slight differences in the cases of semi-cloudy day and overcast day. Differences between HKO measurements at KP and KSC sites are due to the inhomogeneity of solar radiation probably related to different atmospheric conditions among this region. An investigation of this inhomogeneity is presented in Section 4.1.

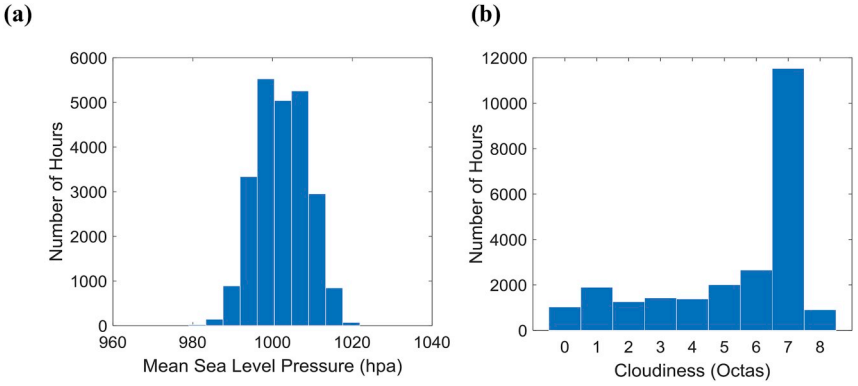

Fig. C.1. The histograms of hourly averaged sea-level pressure in **(a)** and cloudiness in **(b)** between 8:00 h and 18:00 h from HKO measurements from 2009 to 2014.

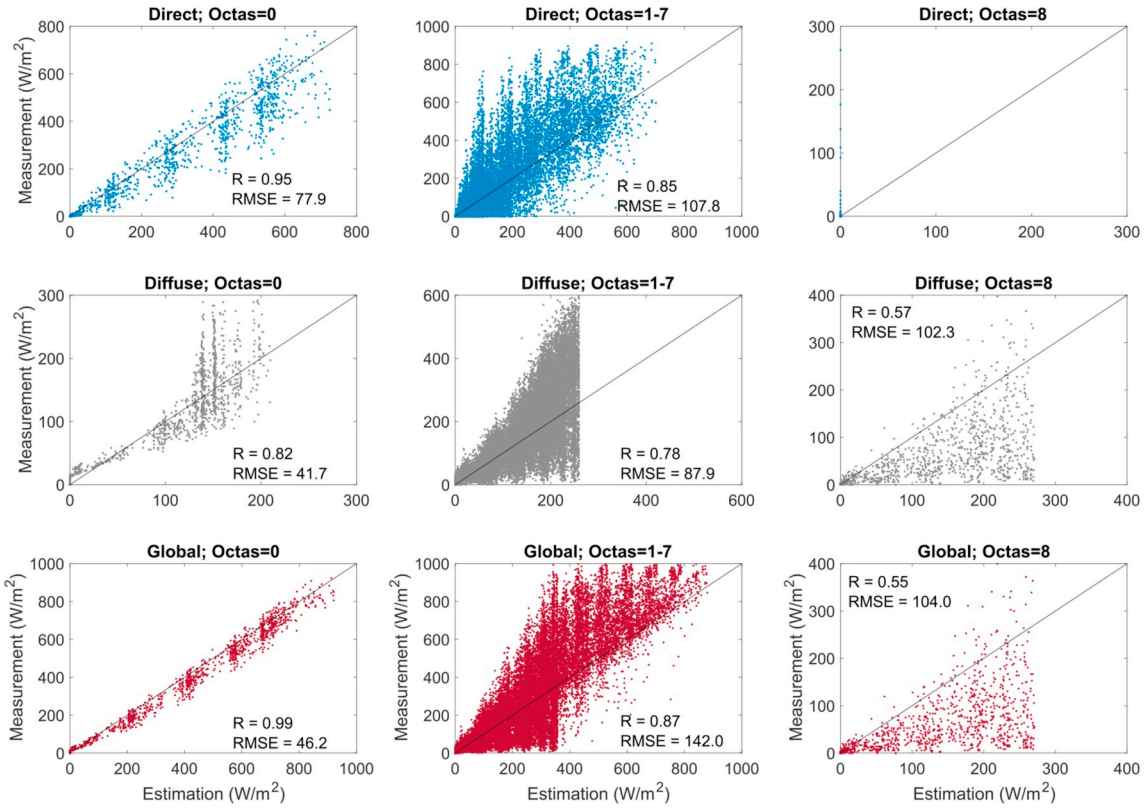

Fig. C.2. Scatter plots between the calculated free-horizon hourly solar irradiance and HKO measurements at the site of King's Park. The plots are grouped by hourly solar irradiation, including direct and diffuse components, under different cloud coverages in terms of octas as measured for six years by HKO from 2009 to 2014.

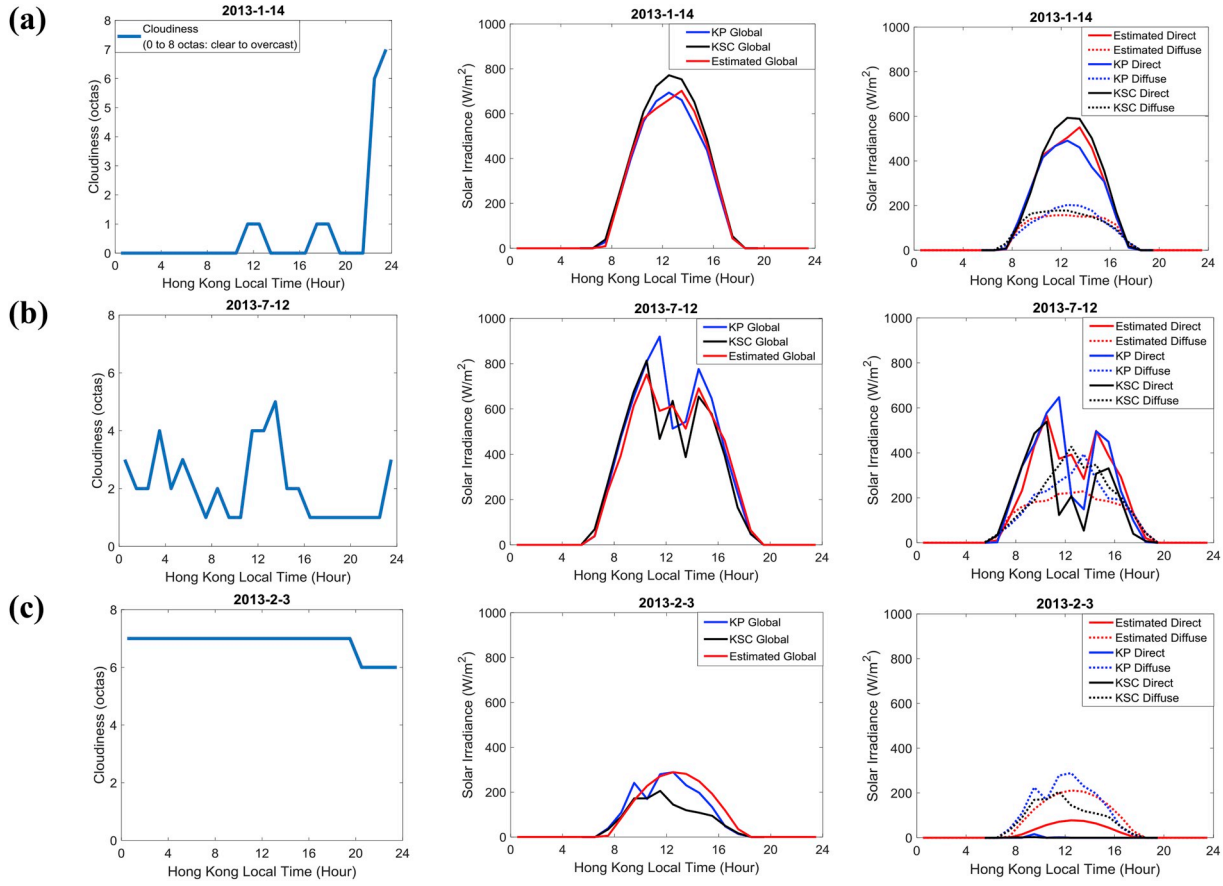

Fig. C.3. Comparison of estimated all-sky irradiance and HKO measurement of hourly global, direct, and diffuse solar irradiance for three different cloudiness example days: **(a)** A clear day (octas = 0–1); **(b)** A semi-cloudy day (octas = 2–6); **(c)** A cloudy day (octas = 7–8).

References

[1] T.R. Oke, The urban energy balance, Prog. Phys. Geogr. Earth Environ. 12 (4) (Dec. 1988) 471–508.

[2] K. Oleson, Contrasts between urban and rural climate in CCSM4 CMIP5 climate change scenarios, J. Clim. 25 (5) (Aug. 2011) 1390–1412.

[3] R. Sanusi, D. Johnstone, P. May, S.J. Livesley, Street orientation and side of the street greatly influence the microclimatic benefits street trees can provide in summer, J. Environ. Qual. 45 (1) (02/01 2016) 167–174.

[4] J.A. Jakubiec, C.F. Reinhart, A method for predicting city-wide electricity gains from photovoltaic panels based on LiDAR and GIS data combined with hourly Daysim simulations, Sol. Energy 93 (Jul. 2013) 127–143.

[5] T.R. Oke, The energetic basis of the urban heat island, Q. J. R. Meteorol. Soc. 108 (455) (Jan. 1982) 1–24.

[6] M.D. Farrar, et al., Efficacy of a dose range of simulated sunlight exposures in raising vitamin D status in South Asian adults: implications for targeted guidance on sun exposure, Am. J. Clin. Nutr. 97 (6) (Jun. 2013) 1210–1216.

[7] L.E. Rhodes, et al., Recommended summer sunlight exposure levels can produce sufficient (≥20ngml−1) but not the proposed optimal (≥32ngml−1) 25(OH)D levels at UK latitudes, J. Invest. Dermatol. 130 (5) (May 2010) 1411–1418.

[8] A.R. Webb, Considerations for lighting in the built environment: non-visual effects of light, Energy Build. 38 (7) (Jul. 2006) 721–727.

[9] H. Akbari, M. Pomerantz, H. Taha, Cool surfaces and shade trees to reduce energy use and improve air quality in urban areas, Sol. Energy 70 (3) (Jan. 2001) 295–310.

[10] S. Thorsson, F. Lindberg, J. Björklund, B. Holmer, D. Rayner, Potential changes in outdoor thermal comfort conditions in Gothenburg, Sweden due to climate change: the influence of urban geometry, Int. J. Climatol. 31 (2) (2010) 324–335.

[11] A. Chow, A.S. Fung, S. Li, GIS modeling of solar neighborhood potential at a fine spatiotemporal resolution, Buildings 4 (2) (May 2014) 195–206.

[12] F.-Y. Gong, Z.-C. Zeng, F. Zhang, X. Li, E. Ng, L.K. Norford, Mapping sky, tree, and building view factors of street canyons in a high-density urban environment, Build. Environ. 134 (Apr. 2018) 155–167.

[13] D. Fröhlich, A. Matzarakis, Modeling of changes in thermal bioclimate: examples based on urban spaces in Freiburg, Germany, Theor. Appl. Climatol. 111 (3–4) (Feb. 2013) 547–558.

[14] E. Krüger, P. Drach, R. Emmanuel, O. Corbella, Urban heat island and differences in outdoor comfort levels in Glasgow, UK, Theor. Appl. Climatol. 112 (1–2) (Apr. 2013) 127–141.

[15] R. Carrasco-Hernandez, A.R.D. Smedley, A.R. Webb, Using urban canyon geometries obtained from Google Street View for atmospheric studies: potential applications in the calculation of street level total shortwave irradiances, Energy Build. 86 (Supplement C) (Jan. 2015) 340–348.

[16] X. Li, C. Ratti, I. Seiferling, Quantifying the shade provision of street trees in urban landscape: a case study in Boston, USA, using Google Street View, Landsc. Urban Plann. 169 (Supplement C) (Jan. 2018) 81–91.

[17] J. Liang, et al., Automatic sky view factor estimation from street view photographs—a big data approach, Rem. Sens. 9 (5) (Apr. 2017) 411.

[18] A. Middel, J. Lukasczyk, R. Maciejewski, M. Demuzere, M. Roth, Sky View Factor footprints for urban climate modeling, Urban Clim. 25 (Sep. 2018) 120–134.

[19] X. Li, C. Ratti, Mapping the spatio-temporal distribution of solar radiation within street canyons of Boston using Google Street View panoramas and building height model, Landsc. Urban Plann. (Aug. 2018), https://doi.org/10.1016/j.landurbplan.2018.07.011 in press.

[20] Census and Statistics Department, The Government of Hong Kong S. A. R, Population - Overview, Census and Statistics Department, 2016 [Online]. Available: http://www.censtatd.gov.hk/hkstat/sub/so20.jsp , Accessed date: 25 October 2017.

[21] Hong Kong Observatory, The year's weather - 2016, [Online]. Available: http://www.hko.gov.hk/wxinfo/pastwx/2016/ywx2016.htm, (2016) , Accessed date: 27 November 2017.

[22] E. Ng, V. Cheng, Urban human thermal comfort in hot and humid Hong Kong, Energy Build. 55 (Supplement C) (Dec. 2012) 51–65.

[23] C. Yuan, E. Ng, L.K. Norford, Improving air quality in high-density cities by understanding the relationship between air pollutant dispersion and urban morphologies, Build. Environ. 71 (Supplement C) (Jan. 2014) 245–258.

[24] W. Wang, W. Zhou, E.Y.Y. Ng, Y. Xu, Urban heat islands in Hong Kong: statistical modeling and trend detection, Nat. Hazards 83 (2) (Sep. 2016) 885–907.

[25] K.L. Bristow, G.S. Campbell, On the relationship between incoming solar radiation and daily maximum and minimum temperature, Agric. For. Meteorol. 31 (2) (May 1984) 159–166.

[26] S.G. Hodder, K. Parsons, The effects of solar radiation on thermal comfort, Int. J. Biometeorol. 51 (3) (Jan. 2007) 233–250.

[27] J.T. Peterson, E.C. Flowers, Interactions between air pollution and solar radiation, Sol. Energy 19 (1) (Jan. 1977) 23–32.

[28] I.D. Stewart, T.R. Oke, Local climate zones for urban temperature studies, Bull. Am.

Meteorol. Soc. 93 (12) (May 2012) 1879–1900.
[29] Google Maps APIs, Google Street View Image API | Google Street View Image API, *Google Developers*, 2017 [Online]. Available: https://developers.google.com/maps/documentation/streetview/intro , Accessed date: 20 October 2017.
[30] Google Maps APIs, Street View Image Metadata | Google Street View Image API, *Google Developers*, 2017 [Online]. Available: https://developers.google.com/maps/documentation/streetview/metadata , Accessed date: 27 November 2017.
[31] Google Maps APIs, Street View Service | Google Maps JavaScript API, Google Developers, 2017 [Online]. Available: https://developers.google.com/maps/documentation/javascript/streetview , Accessed date: 21 March 2018.
[32] National Renewable Energy Laboratory, MIDC: solar position and intensity (SOLPOS) calculator, [Online]. Available: https://midcdmz.nrel.gov/solpos/solpos.html, (2018) , Accessed date: 29 March 2018.
[33] Hong Kong Observatory, 24-hour time series of mean sea level pressure in Hong Kong, [Online]. Available http://www.hko.gov.hk/wxinfo/ts/display_element_pp_e.htm, (2003) , Accessed date: 13 May 2018.
[34] D.H.W. Li, J.C. Lam, A study of atmospheric turbidity for Hong Kong, Renew. Energy 25 (1) (Jan. 2002) 1–13.
[35] Hong Kong Observatory, King's Park meteorological station, [Online]. Available: http://www.hko.gov.hk/wxinfo/aws/kpinfo.htm, (2003) , Accessed date: 21 March 2018.
[36] Hong Kong Observatory, Climate Change in Hong Kong - Cloud Amount, Solar Radiation and Evaporation, (2018) [Online]. Available: http://www.hko.gov.hk/climate_change/obs_hk_cloud_e.htm , Accessed date: 24 May 2018.
[37] H. Zhao, J. Shi, X. Qi, X. Wang, J. Jia, Pyramid Scene Parsing Network, (Dec. 2016) ArXiv161201105 Cs.
[38] B. Zhou, H. Zhao, X. Puig, S. Fidler, A. Barriuso, A. Torralba, Semantic Understanding of Scenes through the ADE20K Dataset, (Aug. 2016) ArXiv160805442 Cs.
[39] T.R. Oke, Street design and urban canopy layer climate, Energy Build. 11 (1) (Mar. 1988) 103–113.
[40] A. Matzarakis, F. Rutz, H. Mayer, Modelling radiation fluxes in simple and complex environments: basics of the RayMan model, Int. J. Biometeorol. 54 (2) (Mar. 2010) 131–139.
[41] E. Erell, D. Pearlmutter, D. Boneh, P.B. Kutiel, Effect of high-albedo materials on pedestrian heat stress in urban street canyons, Urban Clim. 10 (Dec. 2014) 367–386.
[42] K.N. Liou, An Introduction to Atmospheric Radiation, Elsevier, 2002.
[43] J. Ross, Incident radiation, The Radiation Regime and Architecture of Plant Stands, Springer Netherlands, Dordrecht, 1981, pp. 159–174.
[44] A. Matzarakis, F. Rutz, H. Mayer, Modelling radiation fluxes in simple and complex environments—application of the RayMan model, Int. J. Biometeorol. 51 (4) (Mar. 2007) 323–334.
[45] G. Jendritzky, Methodik zur räumlichen Bewertung der thermischen Komponente im Bioklima des Menschen: fortgeschriebenes Klima-Michel-Modell. na, (1990).
[46] F. Kasten, A.T. Young, Revised optical air mass tables and approximation formula, Appl. Opt. 28 (22) (Nov. 1989) 4735.
[47] F. Kasten, The linke turbidity factor based on improved values of the integral Rayleigh optical thickness, Sol. Energy 56 (3) (Mar. 1996) 239–244.
[48] P. Valko, Die Himmelsstrahlung in ihrer Beziehung zu verschiedenen Parametern, Arch. Für Meteorol. Geophys. Bioklimatol. Ser. B 14 (3–4) (Mar. 1966) 336–359.
[49] Hong Kong Observatory, Direct and diffuse solar radiation information added to Observatory's website, [Online]. Available: http://www.hko.gov.hk/press/D4/pre20100401e.htm, (2012) , Accessed date: 22 February 2018.
[50] LI-COR Biosciences, Principles of radiation measurement, [Online]. Available: https://licor.app.boxenterprise.net/s/liuswfuvtqn7e9loxaut, (2015) , Accessed date: 13 June 2018.
[51] Hong Kong Observatory, 24-hour time series of solar radiation, [Online]. Available: http://www.hko.gov.hk/wxinfo/ts/display_element_solar_e.htm, (2003) , Accessed date: 12 May 2018.
[52] Hong Kong Observatory, Climate of Hong Kong, [Online]. Available: http://www.weather.gov.hk/cis/climahk_e.htm, (2010) , Accessed date: 22 June 2018.
[53] R. Giridharan, S.S.Y. Lau, S. Ganesan, B. Givoni, Lowering the outdoor temperature in high-rise high-density residential developments of coastal Hong Kong: the vegetation influence, Build. Environ. 43 (10) (Oct. 2008) 1583–1595.
[54] F. Ali-Toudert, H. Mayer, Numerical study on the effects of aspect ratio and orientation of an urban street canyon on outdoor thermal comfort in hot and dry climate, Build. Environ. 41 (2) (Feb. 2006) 94–108.
[55] C.Y. Jim, The status and prospects of urban trees in Hong Kong, Landsc. Urban Plann. 14 (Jan. 1987) 1–20.
[56] T.E. Morakinyo, F.-Y. Gong, Z. Tan, K.K.-L. Lau, C. Ren, E. Ng, Pilot study of urban green space configuration, trees distribution, species diversity and users' assessment in Hong Kong, Urban For. Urban Green. (2018) submitted for publication.
[57] J. Konarska, F. Lindberg, A. Larsson, S. Thorsson, B. Holmer, Transmissivity of solar radiation through crowns of single urban trees—application for outdoor thermal comfort modelling, Theor. Appl. Climatol. 117 (3–4) (Aug. 2014) 363–376.